NOTICE

AVIS

The quality of this microform is heavily dependent upon the quality of the original thesis submitted for microfilming. Every effort has been made to ensure the highest quality of reproduction possible.

If pages are missing, contact the university which granted the degree.

Some pages may have indistinct print especially if the original pages were typed with a poor typewriter ribbon or if the university sent us an inferior photocopy.

Previously copyrighted materials (journal articles, published tests, etc.) are not filmed.

Reproduction in full or in part of this microform is governed by the Canadian Copyright Act, R.S.C. 1970, c. C-30.

La qualité de cette microforme dépend grandement de la qualité de la thèse soumise au microfilmage. Nous avons tout fait pour assurer une qualité supérieure de reproduction.

S'il manque des pages, veuillez communiquer avec l'université qui a conféré le grade.

La qualité d'impression de certaines pages peut laisser à désirer, surtout si les pages originales ont été dactylographiées à l'aide d'un ruban usé ou si l'université nous a fait parvenir une photocopie de qualité inférieure.

Les documents qui font déjà l'objet d'un droit d'auteur (articles de revue, tests publiés, etc.) ne sont pas microfilmés.

La reproduction, même partielle, de cette microforme est soumise à la Loi canadienne sur le droit d'auteur, SRC 1970, c. C-30.

Canada

THE UNIVERSITY OF ALBERTA

Physics of the Marine Ice Accretion Process
  i) Spreading and Freezing of Saltwater drops
  ii) Mass Loss due to Splashing on a Wet Accretion

by

Eric Obreiter

A THESIS

SUBMITTED TO THE FACULTY OF GRADUATE STUDIES AND RESEARCH

IN PARTIAL FULBILMENT OF THE REQUIREMENTS FOR THE DEGREE

OF MASTER OF SCIENCE

DEPARTMENT OF MECHANICAL ENGINEERING

EDMONTON, ALBERTA
Fall, 1987

THE UNIVERSITY OF ALBERTA

RELEASE FORM

NAME OF AUTHOR: Eric Obreiter

TITLE OF THESIS: Physics of the Marine Ice Accretion Process i) Spreading and Freezing of Saltwater Drops ii) Mass Loss due to Splashing on a Wet Accretion.

DEGREE: Master of Science
YEAR THIS DEGREE GRANTED: Fall, 1987

(SIGNED) _Eric Obreiter_

PERMANENT ADDRESS:

1716 - 111th Ave. S.W.
Calgary, Alberta
CANADA   T2W-1R5

DATE: _June 19_ 1987

THE UNIVERSITY OF ALBERTA
FACULTY OF GRADUATE STUDIES AND RESEARCH

The undersigned certify that they have read, and
recommend to the Faculty of Graduate Studies and Research
for acceptance, a thesis entitled

Physics of the Marine Ice Accretion Process
i) Spreading and Freezing of Saltwater drops
ii) Mass Loss due to Splashing on a Wet Accretion

submitted by Eric Obreiter in partial fulfilment of the

requirements for the degree of Master of Science.

_____
(Supervisor)

_____

_____

Date: _____June 19_____87

ABSTRACT

The purpose of this study was to examine several physical phenomenona applicable to the modelling of marine ice accretions. Of particular interest were the effects of the water loss associated with the splashing of drops on a wet accretion and the influence of salinity, surface temperature, drop diameter and impact velocity on the spreading and freezing of drops on cold dry surfaces.

In order to examine the latter phenomenon, an experimental investigation of the impact, spreading and freezing of large drops was undertaken. The investigation utilized large fresh and saltwater drops with diameters ranging from 1.1 to 2.4 mm, impacting at 4.0 to 4.8 m/s on copper, stainless steel, glass, plexiglass and ice surfaces maintained at -10 and -20°C.

To study the effect of water loss, resulting from the splashing of drops on a wet accretion, a computer model was used to look at the mechanics of droplet motion, in particular the trajectories of the small droplets generated by the splashing. The primary purpose was to quantify the mass (i.e. droplets) that can be permanently lost from the surface of a wet accretion as a result of the splashing phenomenon.

ACKNOWLEDGEMENT

Finally, I would like to direct the biggest thanks of all to my wife Sandy, for bearing with me.

TABLE OF CONTENTS

ix

LIST OF FIGURES

LIST OF PLATES

NOMENCLATURE

Symbol		Units
a	acceleration	$[m^2/s]$
A	area	$[m^2]$
Ang_c	drop velocity vector from cylinder surface	[deg]
Ang_d	drop position from stagnation line	[deg]
Ang_{re}	Re-Impact Angle	[deg]
c	specific heat capacity of water	$[J/kg \cdot {}^{\circ}C]$
c_p	constant pressure specific heat capacity	$[J/kg \cdot {}^{\circ}C]$
c_v	constant volume specific heat capacity	$[J/kg \cdot {}^{\circ}C]$
C_{drag}	coefficient of drag	
D	diameter	[m]
DIF	diffusivity of water vapor in air	$[m^2/s]$
E	emissivity	dimensionless
f	Sherwood number	dimensionless
F	force	[N]
G_i	rate of growth of an ice layer	[W]
h	convective heat transfer coefficient	$[W/m^2 \cdot {}^{\circ}C]$
H	distance	[m]
K or k	thermal conductivity	$[W/m \cdot {}^{\circ}C]$
KE	kinetic energy	[J]
l_f	latent heat of fusion	[J/kg]
l_v	latent heat of vaporization	[J/kg]
m	mass	[kg]
Nu	Nusselt number	dimensionless
P	pressure	[Pa]

Symbol		Units
Pr	Prandtl number	dimensionless
R	specific gas constant	$[J/kg \cdot k]$
Re	Reynolds number	dimensionless
S	salinity	$[g/kg]$
Sc	Schmidt number	dimensionless
SE	surface energy	$[J]$
S.F.	spreading factor	dimensionless
t	time	$[s \text{ or } ms]$
T	temperature	$[^{O}C \text{ or } k]$
V	velocity	$[m/s]$
We #	Impact Weber Number	dimensionless
y(t)	thickness of ice layer	$[\mu m]$
X,Y	position of drop	$[m]$
σ	Stefan-Boltzman constant	$[J/m^2 \cdot s \cdot k]$
ρ	density	$[kg/m^3]$
μ	dynamic viscosity of air	$[kg/m \cdot s]$
δR	thickness of spread out drop	$[\mu m]$
α	thermal diffusivity	$[m^2/s]$
γ	surface tension coefficient	$[dyne/cm]$
ψ	stream function	$[m^2/s]$

Subscripts

a	air
c	cylinder or cooling
d	drop
f	freezing
final	final value
i	ice or initial
im	impact
max	maximum value
PT	constant pressure: moist air
s	surface or spreading
T	total
v	vapor
w	water
a/w	air-water interface

CHAPTER 1

INTRODUCTION

1.1 Background Information

With the recent upswing in offshore activities in northern waters has come an increased emphasis on the marine icing phenomenon. The accretion of ice on marine structures (i.e. ships and drilling rigs) produces increased static and wind generated loads on the structures, that can result in potentially hazardous situations. The primary concerns are the instability of floating structures and the possibility of structural damage to stationary and floating structures.

The most dangerous and primary cause of marine ice accretions is the freezing of the sea spray generated by impacting waves. Over a period of several days during a storm in 1979, the semi-submersible drilling rig Ocean Bounty accumulated an estimated 500 tons of ice (Minsk, 1984). Although this load did not damage the structure, it was potentially hazardous and it became necessary to jettison drilling mud as a precaution to maintain stability. Plate 1.1 illustrates the ice accumulation on a small Dutch tanker, "Anna Broere" which ran aground near Cape Rozewie (Poland) in the southern Baltic Sea, January 1, 1979.
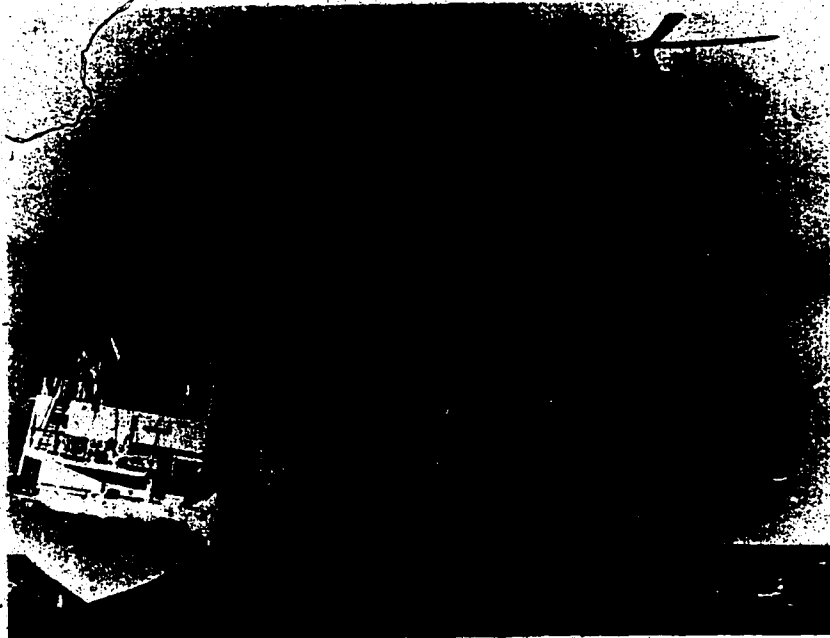
PLATE 1.1   Ice accumulation on a small Dutch Tanker, the
            "Anna Broere", which ran aground near Cape
            Rozewie (Poland southern Baltic sea), Jan.1,
            1979. Photo: Paul Zakrzewski.

PLATE 1.2   Removal of ice accretion from a ship using a
            wooden hammer.

1.2 Modelling

Of particular interest to the marine icing phenomenon has been the development of marine icing "models" that can be used to predict or forecast ice accretion rates for a given set of meteorological, accretion and physical parameters. Such models could aid in the design of marine structures by predicting the mass of accreted ice, which in turn is needed to determine any increased static and/or wind-generated loads. The operator of a marine structure could also use the models to forecast potentially hazardous conditions, and take preventive action if possible. The marine icing models currently available have been developed primarily from two different perspectives, those based on observations (i.e. empirical) and those that are analytical in nature, although the distinction is not always clear.

1.3 Empirical Models

Mertins (1968) developed a series of marine forecasting nomograms to forecast ice accretion rates on ships in the North Atlantic. These nomograms were developed through comparison of environmental parameters with ship icing reports and included the effect of the most important environmental factors, namely air temperature, wind speed and sea temperature. Wise and Comiskey (1980) and Comiskey et. al. (1984) developed nomograms, based on Mertins' original work, to forecast

superstructure icing in Alaskan waters. Pease and Comiskey (1985), using data from ship icing incidents in Alaskan waters, also developed marine nomograms to forecast the most severe cases of marine icing.

The major shortcoming of these empirical models, is that since they are based on specific icing data, generalization to different marine structures and meteorological conditions has met with limited success. As well, the majority of the observations correspond to the icing of ships, primarily smaller vessels and the applicability to large stationary structures (e.g. drilling platforms) is not obvious. As a result, increased emphasis has been placed on the development of analytical models which ideally could be used to predict ice accretion mass and possible shape, for arbitrarily shaped accretion surfaces and a wide range of environmental conditions.

1.4 Analytical Models

Analytical models attempt to model the physics of the icing process. The basic algorithm involves determining the mass flux that is accreted (i.e. collision efficiency) and how much of the accreted mass freezes or if it all freezes, the accretion surface temperature via the steady state heat balance at surface of the accretion. The collision efficiency is defined as the fractional mass in a swept out volume that is accreted on a surface.

Horjen, et. al. (1984), Stallabrass (1980) and Kachurin, et. al. (1974) have all developed analytical marine icing model using the same "basic" algorithm, although the details of their formulations are somewhat different. Previously, analytical models have been developed that predict the accumulation of ice under "atmospheric" icing conditions. In developing these analytical models the authors must make simplifying assumptions to keep the models practical. These simplifying assumptions are generally derived from an understanding of the basic physics of the appropriate accretion process.

Since the basic physics of the marine icing process are presently not well understood, the authors take a "black box" approach, ignoring the details of the kinematic and thermodynamic processes of the single drops in terms of the overall accretion process. Although it might be possible to develop a marine icing algorithm along the same lines as an atmospheric icing model, the conditions typically associated with the marine icing situation would prevent the use of the simplifing assumptions based on atmospheric icing conditions. The major differences between marine and atmospheric icing conditions are large drops generally not in kinematic or thermodynamic equilibrium with the air, intermittent periods of no icing and salinity. In order to improve analytical marine icing models, the modellers must develop

a better understanding of the basic physics of the marine ice accretion process.

1.5 Present Investigation

The present investigation was undertaken in order to examine some of the basic physics of the marine ice accretion process, with particular interest in the spreading and freezing of large saline drops on cold dry surfaces and the splashing of drops on a liquid layer. Towards this end an experimental investigation was under taken to determine the importance of salinity, surface temperature, drop size and velocity on the spreading of single drops on cold dry surfaces. In addition the effect of heat transfer and freezing on this spreading process was also examined. Of primary importance was the relationship between the spreading and freezing of the single drops to the overall marine ice accretion process.

A further analytical investigation was undertaken in order to examine the kinematics of the splashing process in relationship to the splashing of drops on a liquid surface in a wet accretion. Plate 1.3 illustrates the "splash" produced when a 2.4 mm diameter drop impacts with a velocity of 4.8 m/s (V_{im}) on a layer of water. The primary purpose of this investigation was to quantify the mass loss associated with the splashing of drops on a "wet" (i.e. partially unfrozen) accretion, typical of the marine icing situation.
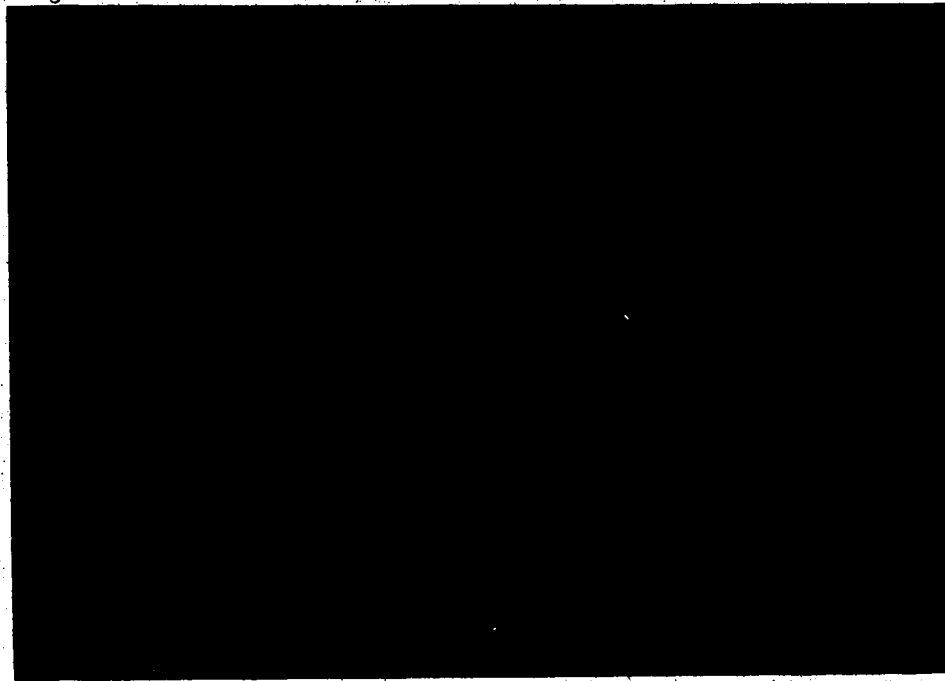
PLATE 1.3   A photograph of the small drops "shed" from
            the crown of water as a result of the
            splashing of a 2.4 mm diameter drop on a
            layer of water (V_{im} = 4.8 m/s).

CHAPTER 2

EXPERIMENTAL APPARATUS AND TEST PROCEDURES

In order to examine the spreading and freezing of large drops on cold dry surfaces, an experimental set-up was developed to maintain the surface temperature and record the spreading process. This was accomplished through the use of high speed photographic and video techniques which effectively "slowed" the motion of the spreading drop. Additional tests were also performed to determine the "freezing time" of the drops.

2.1 The Cold Room

The majority of the experimental tests were conducted in a Foster refrigerated cold room. The cold room is one of three cold rooms located in the Mechanical Engineering Building at the University of Alberta. The cold room has a floor area of 4 m^2 and an interior height of 2.15 meters. The forced air cooling unit is capable of maintaining the temperature in the cold room between -5 and -23 $\pm$ 1°C.

Figure 2.1 is a schematic of the equipment and experimental set-up located in this cold room. The major components of the set-up are the drop source (single drop generator), the drop timing circuit, a 35 mm Nikon camera and a strobotac. The drop source was used to produce single drops, ranging from 1.1 to 2.4 mm in diameter. A detailed description of the drop source can be found in
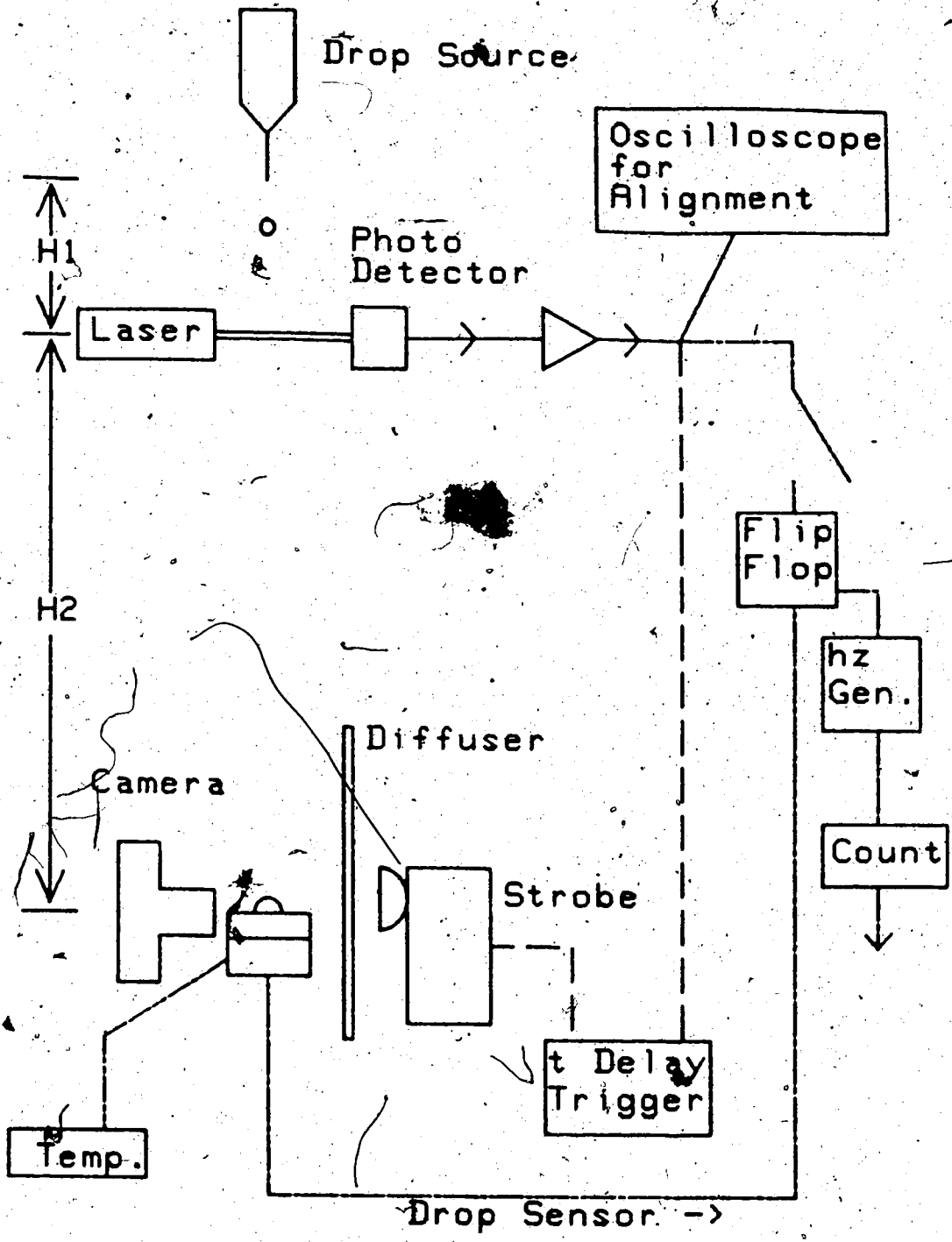
FIGURE 2.1 Schematic of the cold room set-up and
equipment used in the photographing of
spreading drops on cold surfaces.

Section 2.2.3. The drops fell a total of 168.5 cm before impacting on the cold test surfaces. Located 70 cm (H1) below the drop source was a Laser (Hughes, Model 3221H-C) and a Photo Detector. The Photo Detector was used to detect the drops at the instant they had fallen the 70 cm from the drop source. The electrical signal from the Photo Detector could then be used in the drop timing circuit to determine the time required for the drop to fall the additional 98.5 cm (H2). In order to record the spreading of the drops a 35 mm single lens reflex camera complete with a 55 mm macro lens and a 68 mm extension tube was focused on the impact surface. This combination of the lens and extension tube produces an image to subject size ratio of 1.24. Located directly opposite the camera was a light diffuser (Lexan Sheet) and a General Radio Type 1531A Strobotac (Light source). The photo detector output was used to initiate a timing circuit which caused a single flash of light to be emitted from the strobotac. The duration of the flash was on the order of several microseconds.

2.2 Drop Production

One of the main thrusts of the experimental study was to determine if salinity produced any significant differences, in terms of the spreading and freezing of water drops on cold dry surfaces. This difference was to be determined through the size (diameter) and the

appropriate times required for the drops to spread and freeze on the cold dry surfaces. Of particular interest in this study were the drops representative of the sea spray generated by wave impacts. This sea spray generally consists of relatively large drops up to several millimeters in diameter. A method of producing consistently sized "single" drops with predictable trajectories had to be developed before any meaningful experimental results could be obtained. The required method shall be referred to as Drop Generation.

2.2.1 Drop Generation

Besides the need for repeatable drop sizes, the photographic techniques employed in this study necessitated two additional drop production requirements. First, the drops had to fall with a controllable and consistent trajectory and second, the rate of drop production had to be no greater than approximately 1 drop/second. These requirements were based strictly on the need to obtain detailed photographs of single drops as they spread on a cold dry surface. The consistent trajectories ensured that the drops fell on the impact surface, at the position corresponding to the focal point of the camera. The maximum drop production rate of 1 drop/sec was needed to prevent multiple photo detector signals or equivalently, multiple film exposures.

The problems associated with producing repeatable drop

diameters have been investigated for many years. As early as 1882, Rayleigh used vibrations to break up a jet of liquid into a stream of regularly spaced drops (Magarvey and Taylor, 1956). To meet all of the special drop production requirements of this present study, several drop production methods were investigated before a suitable method was found.

2.2.2 Methods of Drop Production

Initially, water was allowed to flow through a small stainless steel tube with inner and outer diameters of 0.69 and 1.07 mm, respectively. This method consistently produced drops 2.55 mm in diameter. The theory behind this method of drop production is that the drop will grow at the tip of the tube until its weight is great enough to overcome the surface tension forces, "adhering" the drop to the tip. Lane (1946) showed that to obtain a 1.0 mm diameter drop requires a tube with an outer diameter of 0.02 mm. From a practical point of view, it is not possible to construct and successfully use a 0.02 mm tube to produce 1.0 mm drops.

Several authors (Lane 1946, Reil and Hallett 1969, Samuels and Sparks, 1973 and Cheng and Cross, 1975) have shown that it is possible to obtain uniformly sized drops, by allowing a concentric stream of air to "blow" suspended drops from the tip of a hypodermic needle (Figure 2.2). Changes in the air flow velocity and the flow rate of the

HYPODERMIC
NEEDLE

D_{outer}/D_{inner}

1.65/1.20

1.07/0.69

0.64/0.33

0.35/0.18

50

HIGH
VOLTAGE
SOURCE

GROUNDED PLATE
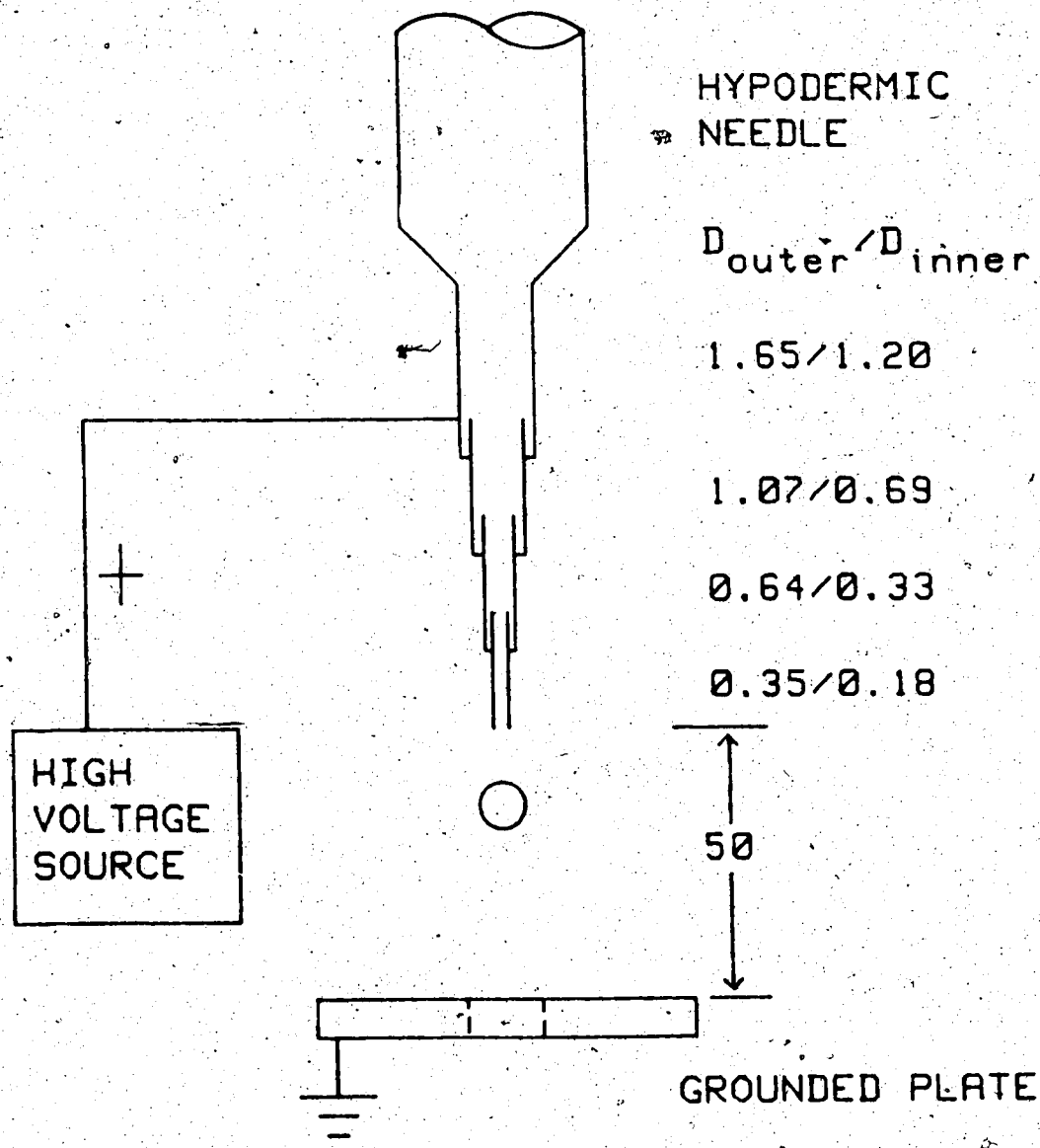
FIGURE 2.2   Dropping Tip used in conjunction with a high
voltage source to produce a range of single,
uniformly sized water drops (all dimensions
are in millimeters).

dropping liquid vary the size and frequency of drop production. However, the range of drop sizes is limited by the tube or tip diameter.

In order to effectively decrease the diameter of the hypodermic needle (dropping tip), a series of stainless steel tubes were "telescoped" down to the final smallest tip diameter (Figure 2.2). This telescoping design served several useful purposes. First the smallest diameter provides an upper limit for the drop size (no airflow to blow the drop from tip). As well, in comparison to a single tube with the smallest diameter, the telescoping reduces the resistance to the flow of water through the tip and provides greater rigidity to the dropping tip.

An actual working model of the concentric air device (Figure 2.3) was constructed, and testing showed it was capable of producing drops ranging from 0.5 to 2.5 mm in diameter using the tip specified in Figure 2.2. The major drawbacks of the device included the difficulties associated with producing repeatable drop trajectories and controlling drop production frequencies. Both of these difficulties had to be overcome to ensure the success of this study. Further work on the device by others, Samuels and Sparks (1973) and Cheng and Cross (1975), indicated that pulsing the air flow could help alleviate the trajectory problems. Although it may have been possible to modify the concentric air device, the complications and sophistication could not be justified for this study. It

Water Flow

Air
Flow

<---- Ground Glass
Joint

Flow
Straighteners

Luer   ------->
Connector
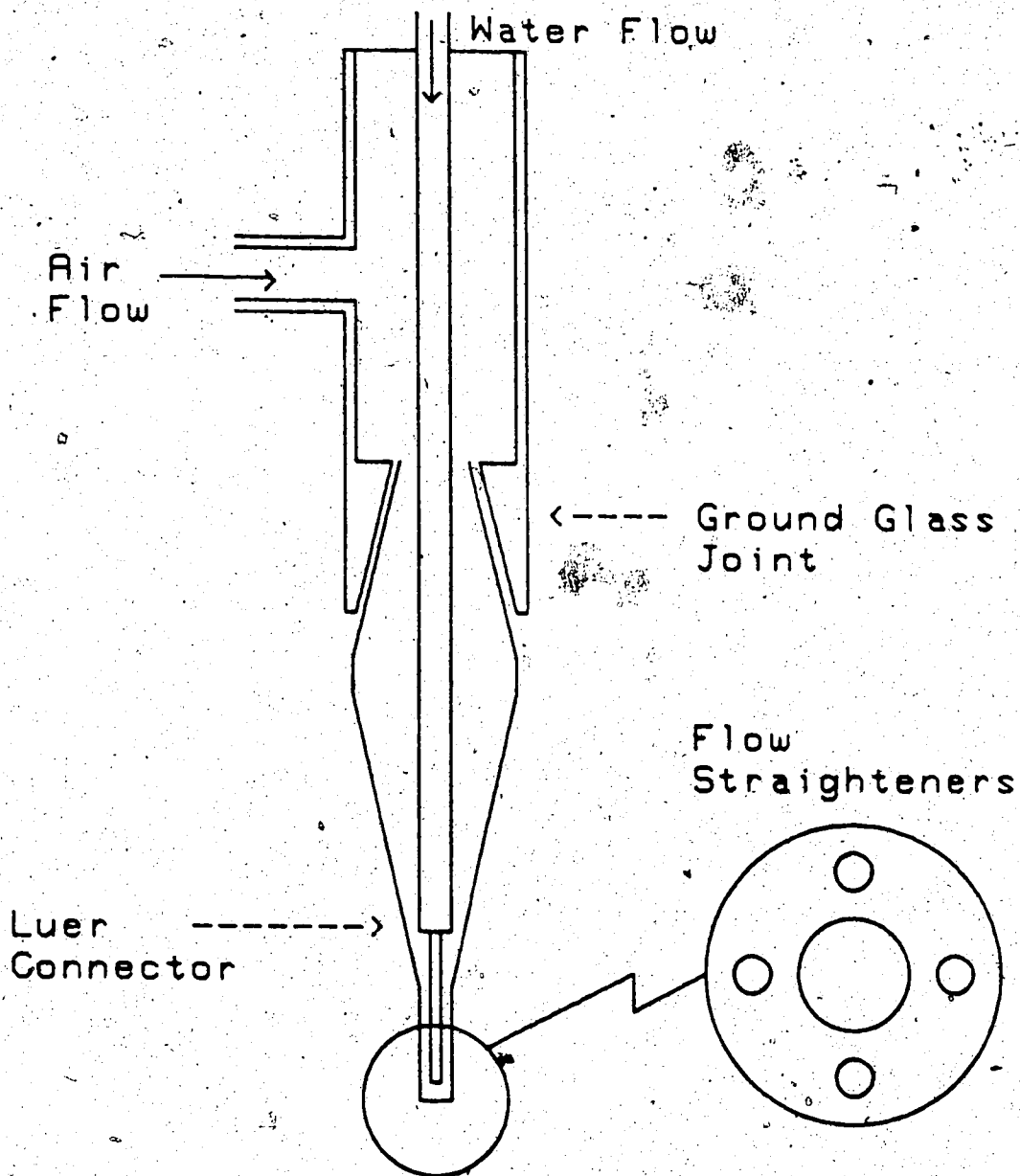
FIGURE 2.3   Schematic of a "Concentric Air" drop
            generator.

was therefore determined that an alternate method be
employed to produce the single drops.

Several other devices were investigated before a
suitable drop producing device was choosen. One such
device is that described by Magarvey and Taylor (1956) and
Wolf (1961), in which a vibrating reed is used to break up
a jet of fluid into smaller drops. The drops produced by
this method are generally very small (<1 mm) and are
produced at a rate much too large to be successfully used
in this study. Abbott and Cannon (1972) and later Cannon
and Grotewold (1980) claimed to be able to produce small
drops one at a time, ranging in diameter from 4 to 130 μm
and 6 μm to 1 mm respectively, using the wire eggression
principle. Simply put, the wire egression principle.
involves pulling a fine wire from the meniscus of a fluid
film at rest. The wire draws a "stream" of fluid from the
surface which breaks off and contracts into a drop.
However, the complexity of this device made it impractical
for use in this study.

2.2.3 High Voltage Drop Production Method

The method finally choosen to produce the desired
range of drop sizes uses the electrostatic force between a
charged drop and a fixed ground to "pull" the drops from
the dropping tip. Raghupathy and Sample (1970) and Ahire
and Kamra (1984) have investigated the production of drops
using high voltage sources and Russo, Withnell and Hieftje

(1981) used the method successfully to produce isolated drops for use in the study of atomization in flames.

The basic set-up for the method is shown in Figure 2.2 and involves charging the drops by applying a high voltage potential to the dropping tip. A ground plate, with a centered hole, is placed at fixed distance below the tip. The dropping liquid being positively charged is "attracted" to the grounded plate. If the water in the tip were uncharged, the water would flow from the tip and a drop would grow on the tip until the weight of the drop was large enough to overcome the surface tension force. If however, the drop is now charged by some known voltage, the "Coulomb" attraction will prevent the drop from growing to its maximum size. Figure 2.4 shows the drop diameter as a function of applied voltage for the particular set-up shown in Figure 2.2. It is of interest to note that once the charged drop has been produced, it is possible to vary its trajectory by allowing the drop to pass through an electric field applied between two parallel plates. However, for this study the resulting drop trajectories produced by the high voltage system were repeatable and did not require the application of an electric field. The minimum size of single discernible drops that can be produced by the high voltage system is a function of the dropping tip and grounded plate dimensions, as well as tip to plate spacing. In the particular set-up used for this study (Figure 2.2), the
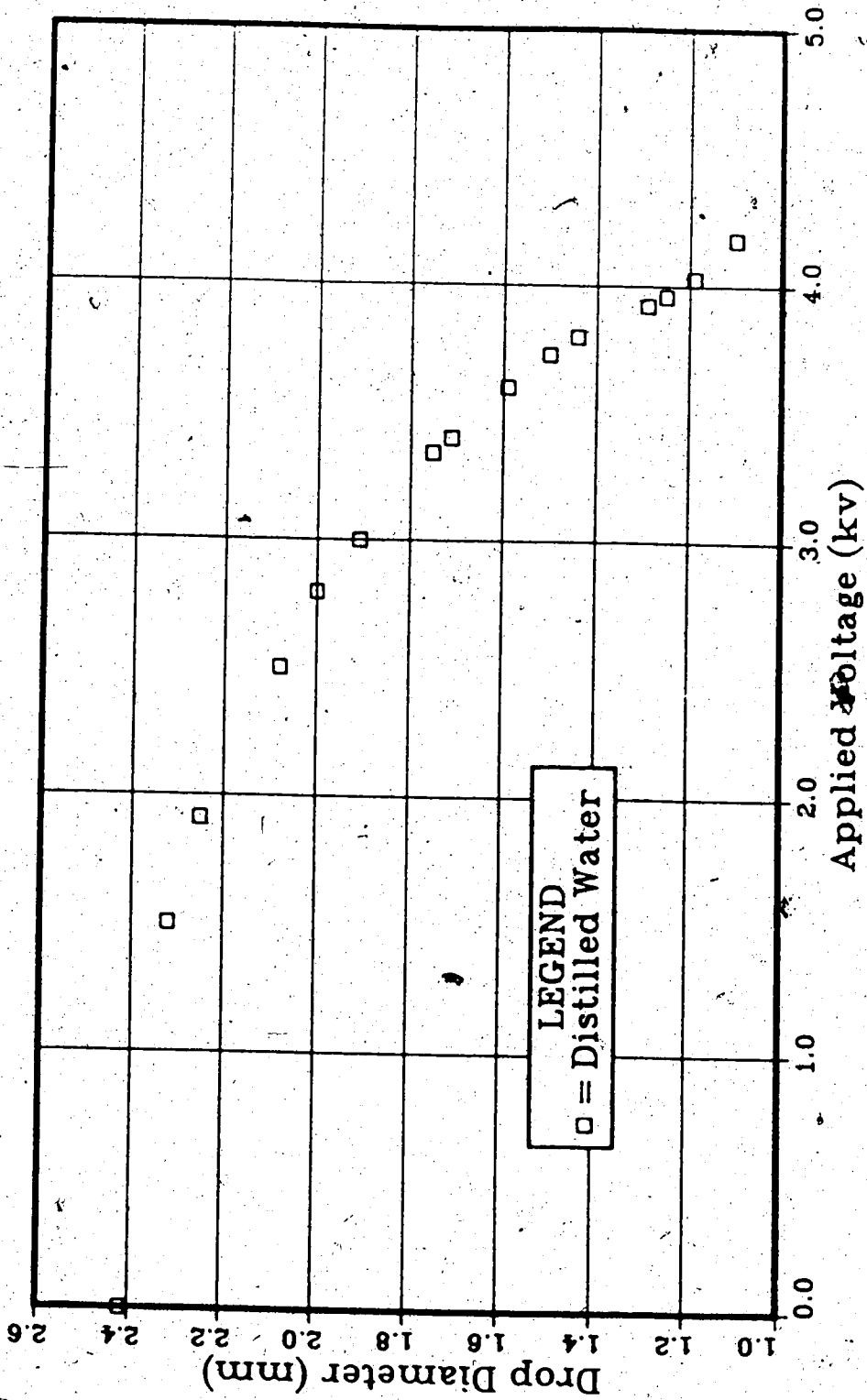
FIGURE 2.4   The diameter of distilled water drops as a function of applied voltage, obtained from the tip illustrated in Figure 2.2.

range of drop diameters obtainable was 1.1 to 2.4 mm. If the applied voltage is increased beyond that required to produce the smallest drops, the drop production mode changes from a "dripping" mode (single drops) to a "spraying" mode, in which numerous randomly sized and very small drops are produced (Ahire and Kamra, 1984).

2.3 Impact Surfaces

In order to ensure a variation in the heat transfer and spreading processes of a drop impacting on a cold dry solid surface, several different impact surfaces were chosen. These included copper, stainless steel, plexiglass, ice and glass. These materials would provide a large range of thermal properties (Table 2.1) and some variation in surface roughness.

The surface of the copper plates was prepared by polishing with 0.05 μm gamma alumina grit. The maximum surface roughness 1.0 μm and centerline average (CLA) roughness 0.1 μm, were measured using a Talysurf Surface Measuring Instrument (The CLA measurement is based on the ASA B46: 1955 standard). The glass, plexiglass and stainless steel plates were utilized with their originally manufactured surfaces intact. The glass and plexiglass surfaces were assummed to be smooth and were replaced if any surface flaws appeared. The surface of the stainless steel plates was protected by removable plastic film. The protected surface was used for all of the experimental

TABLE 2.1   Physical Properties of Impact Surface
             Materials and Water.

Surface Material	ρ Density (kg/m^3)	c - Specific Heat Capacity $(J/kg \cdot {}^{o}C)$	k - Thermal Conductivity $(W/m \cdot {}^{o}C)$
Copper[1] ASTM B152	8941	385	339
Ice[2] @ $0{}^{o}C$	890	2106	2.44
Stainless[1] Steel-304	8027	502	159
Plexiglass[3]	1190	1465	0.376
Water[4] Distilled	1000	4218	0.552
Salt	1025	4070	0.552

1 Metals Handbook, American Society for Metals
2 Pruppacher and Klett (1978)
3 Johnson's Industrial Plastics
4 Mark's Standard, Handbook for Mechanical Engineers

tests and had maximum and centerline roughnesses of 2.5 μm and 0.5 μm, respectively. The ice surfaces were prepared to ensure a high density ice substrate and a smooth impact surface. This was accomplished by slowly freezing samples of warm distilled water and choosing only the samples with minimal quantities of trapped air. The surfaces of the samples were further prepared by melting them on a clean hotplate before refreezing.

The temperature of the surfaces was monitored by thermocouples implanted flush with or just below the surface. Since the method of implanting the thermocouples introduced a local roughness to the impact surface the drops were not allowed to impact at the thermocouple location during any spreading tests. The impact plates (surfaces) were held in place by a small vise mounted on a solid base. The angle of the impact surface could be varied 15° from the horizontal position by pivoting the jaws of the vise.

2.4 Salt Water

In order to examine the influence of salinity on the freezing and spreading of water drops as they impact on cold dry surfaces, it was necessary that a consistent salinity salt water be available. For this reason a synthetic seawater mix under the brand name Rila Marine Mix was choosen to produce the required salt water samples. The mix has the advantage of providing a

chemically defined medium which can be consistently reproduced. A typical chemical analysis of the samples produced from the Rila Marine Mix can be found in Table 2.2. The mix should produce a sample with a salinity close to that of seawater (34.325 g/kg, Assur, 1960) and a specific gravity ranging from 1.020 to 1.025.

The sample solution is prepared by adding 39.943 grams of the dry Rila Marine Mix to each liter of distilled water. The sample was allowed to sit in a closed plastic container for a week to ensure all the salts were dissolved. The sample used for this study had a specific gravity of 1.023 and a salinity of 33 g/kg. Tsurikov (1974) showed that based on the above salinity the corresponding freezing point depression may vary from -1.895 to $-1.917^{\circ}C$, depending on the choice of the semi-empirical formulation. For this study a value of $-1.9^{\circ}C$ was used.

2.5 Drop Velocity and Temperature

As mentioned previously, the large drops in sea spray may not be in thermodynamic or kinematic equilibrium with the surrounding air. In terms of modelling ice accretions under these conditions, it is necessary to calculate the drop temperature and velocity at the instant that the drops impact with an icing surface. Similarly, the temperature and impact velocity of the test drops must be determined to ensure consistency of the experimental

TABLE 2.2   Typical analysis of the salt water produced
from the Rila synthetic seawater mix
(Salinity = 33 ± 0.6 g/kg).

RILA PRODUCTS

P. O. BOX 114   •   TEANECK, N. J.   07666   •   201/836-0855

1-lb. of RILA MARINE MIX when dissolved in 3 gallons of tap water
will produce a solution having the following typical analysis:

	mg/100 ml	ppm
Cl^-	1913	19130
Na^+	1046	10460
$SO_4^=$	260	2600
Mg^{++}	126	1260
Ca^{++}	49	490
K^+	34.8	348
Tris Amino	3.2	32
Br^-	2.7	27
$BO_3^=$	1.2	12
I^-	.897	8.97
Sr^{++}	.350	3.50
Mn^{++}	.050	.50
F^-	.040	.40
Zn^{++}	.020	.20
Fe^{+++}	.010	.10
Co^{++}	.007	.07
Al^{+++}	.003	.03
$MoO_4^=$	.002	.02
Rb^+	.0006	.006
Li^+	.0006	.006
Cu^{++}	.0001	.001

Specific Gravity: approx. 1.025
pH: 8.0 - 8.3
Solubility: complete

measurements.

2.5.1 Drop Impact Velocity

The impact velocity refers to the velocity at which the drops strike the impact surface. To determine the velocity of a water drop falling under the influence of gravity, the gravitional force and the appropriate drag forces must be taken into account. For this reason a "Velocity" program was developed utilizing experimentally and analytically obtained expressions for the drag on a freely falling water drop. A detailed analysis of the development of the program can be found in Appendix A. The program was capable of determining the "instantaneous" drop velocity, as a function of distance fallen or time, by using a stepwise iterative scheme. Since time and distance are both measurable experimental quantities, they may be used in conjunction with the "Velocity" program to ensure an accurate determination of the drop's impact velocity.

Figure 2.5 is a plot of the drop velocity as a function of distance fallen (drop position), as calculated from the "Velocity" program. Given that the initial drop velocity at the dropping tip is known, the impact velocity can be readily determined. However, for the smaller drops produced by the high voltage system, the coulomb attraction results in an "unknown" initial velocity.

Consider two 1.1 mm drops, one with an initial velocity of 1.9 m/s and the other without any initial
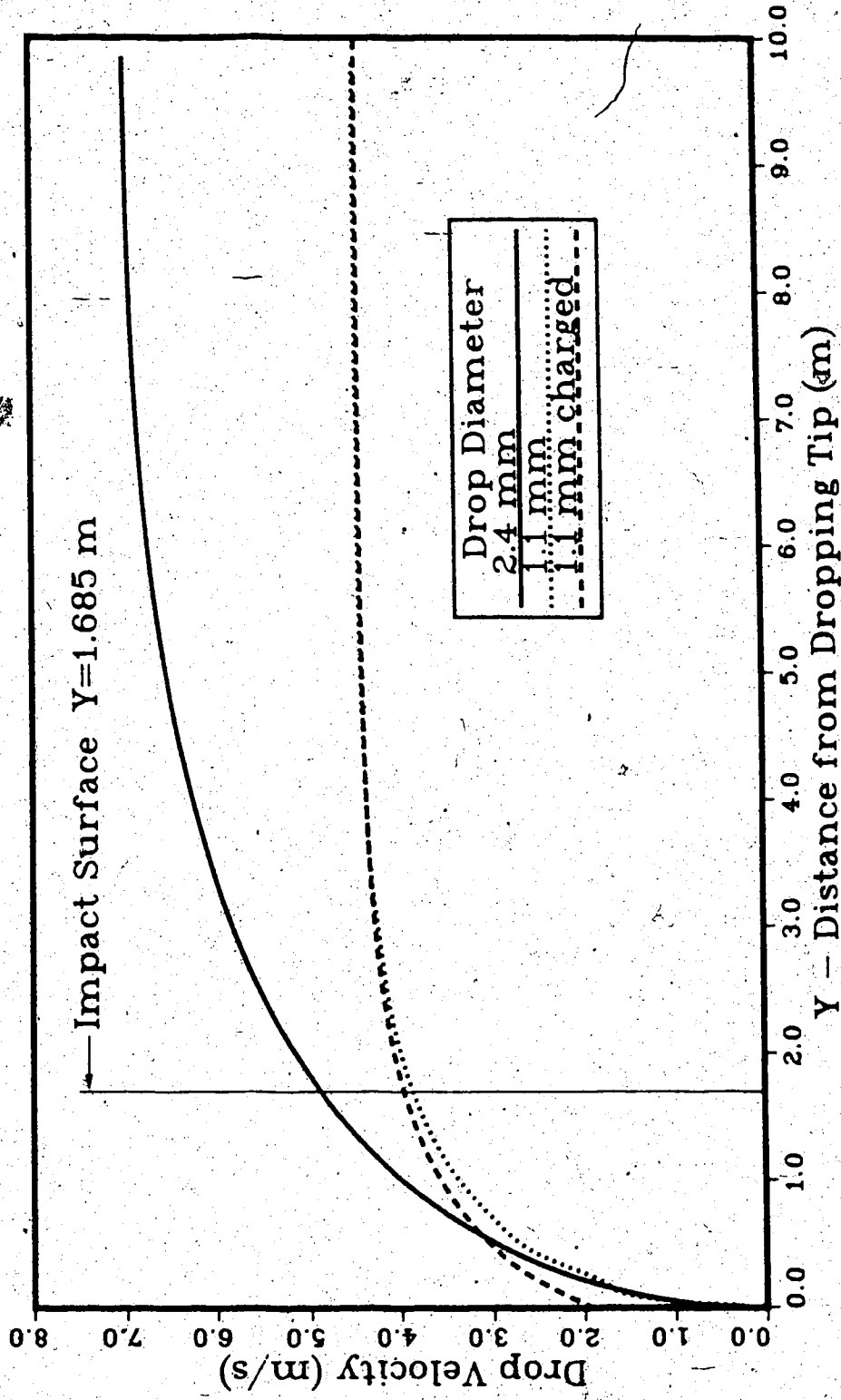
FIGURE 2.5 Effect of the initial velocity of the charged drops on the drop's impact velocity (initial velocity results from coulomb attraction of the high voltage set-up).

velocity. As shown in Figure 2.5 both drops would reach terminal velocity (4.2 m/s) after falling approximately 3 meters. However, at the position of the impact surface, the drop velocities are 4.0 and 3.9 m/s respectively. This illustrates the need to account for the "unknown" initial velocity to ensure the correct impact velocity. This was accomplished through the use of the Drop Timing Circuits.

2.5.2 Drop Timing Circuits

The drop timing circuit, consisting of the laser and photo detector, the time delay generator and the strobotac (Figure 2.1), served two primary purposes. First the circuit was utilized in the photographic technique, as explained in Section 2.6.1, to control the precise triggering of the strobotac used to "freeze" a spreading drop's motion. An appropriate "delay time" was choosen so as to cause the strobotac to flash at the precise moment that the drop touches the impact surface.

Second the circuit provided the time for the drop to fall the distance H2 (98.5 cm) as illustrated in Figure 2.1. This time referred to as the "delay time" was used in conjunction with the "Velocity" program to obtain the impact velocity of the drops produced by the high voltage system, which as a result of the electrostatic force have an unknown initial velocity. The first step in the procedure is to use the "Velocity" program to calculate the position and corresponding velocity of a

freely falling drop as a function of time. Since the drops produced by the high voltage system are "free falling" during the time that they travel the distance H2, it is simply a matter of finding a calculated interval, from the velocity program, in which the drop travels 98.5 cm (H2) in the measured time delay. Since the drops used in this study travel at less than terminal velocity the chosen interval is unique and the endpoint of the interval gives the corresponding impact velocity. Figure 2.6 shows the impact velocities for the 1.1, 1.5 and 2.4 mm diameter drops used in this study. The impact velocities as indicated by the "impact position" were 4.0, 4.4 and 4.8 m/s respectively.

In order to determine this "delay time" for the drops produced by the high voltage source the photo detector output was channeled to a separate timing circuit (Figure 2.7). The signal from the photo detector starts the timing circuit, while a "sensing" plate, placed at the location of the impact surface and responsive to charged drops, stops the circuit. Since the circuit is "counting" the cycles of a 1000 hz signal, the count represents the "delay time" directly in milliseconds.

2.5.3 Drop Temperature

The temperature of the impacting drop was obtained by equating the change in the drop's internal energy to the conductive, radiant and mass transfer modes appropriate to
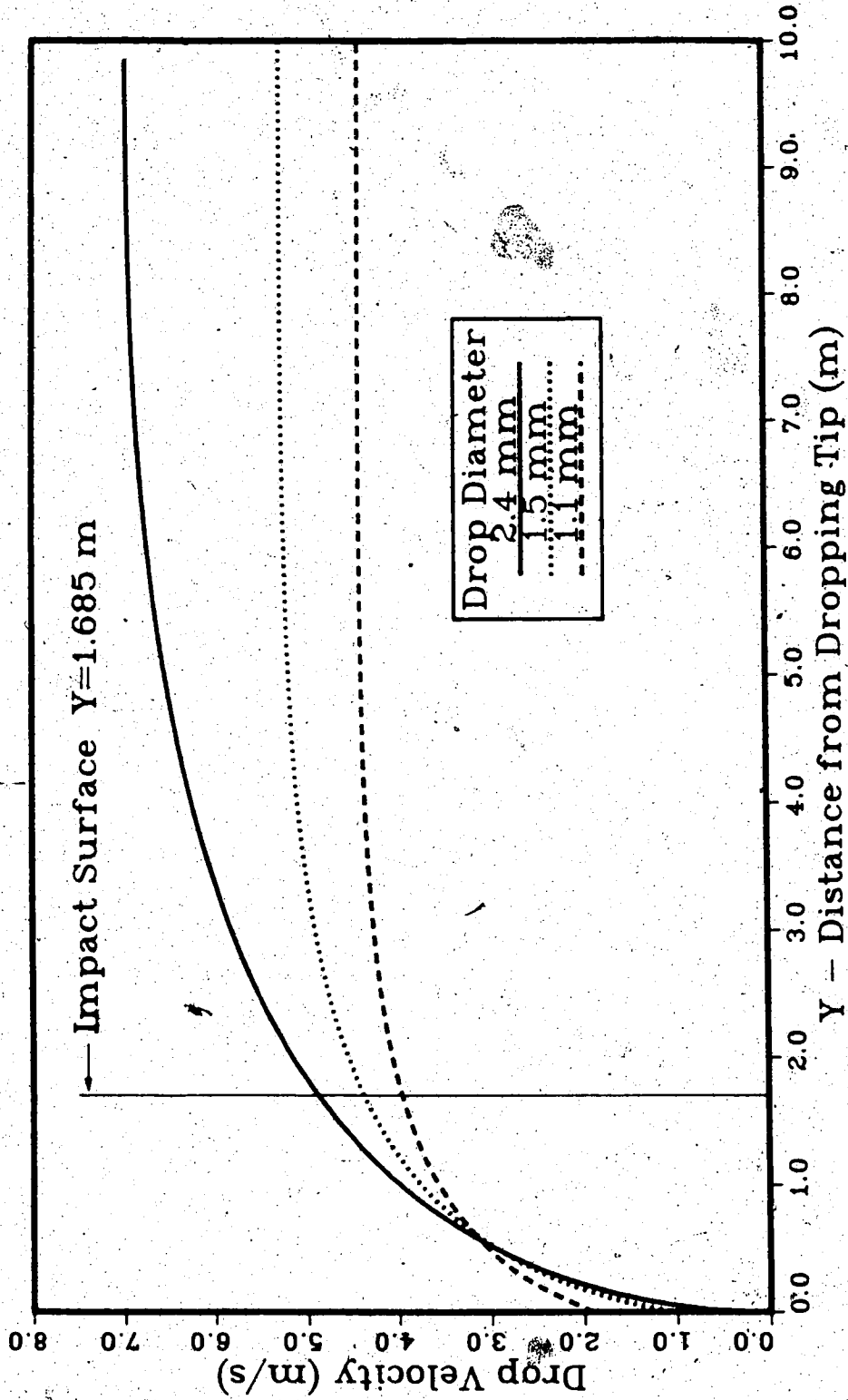
FIGURE 2.6   Drop velocity as a function of distance fallen for drops produced by the high voltage set-up (Figure 2.2). Note that the 2.4 mm drops are not produced using this set-up.
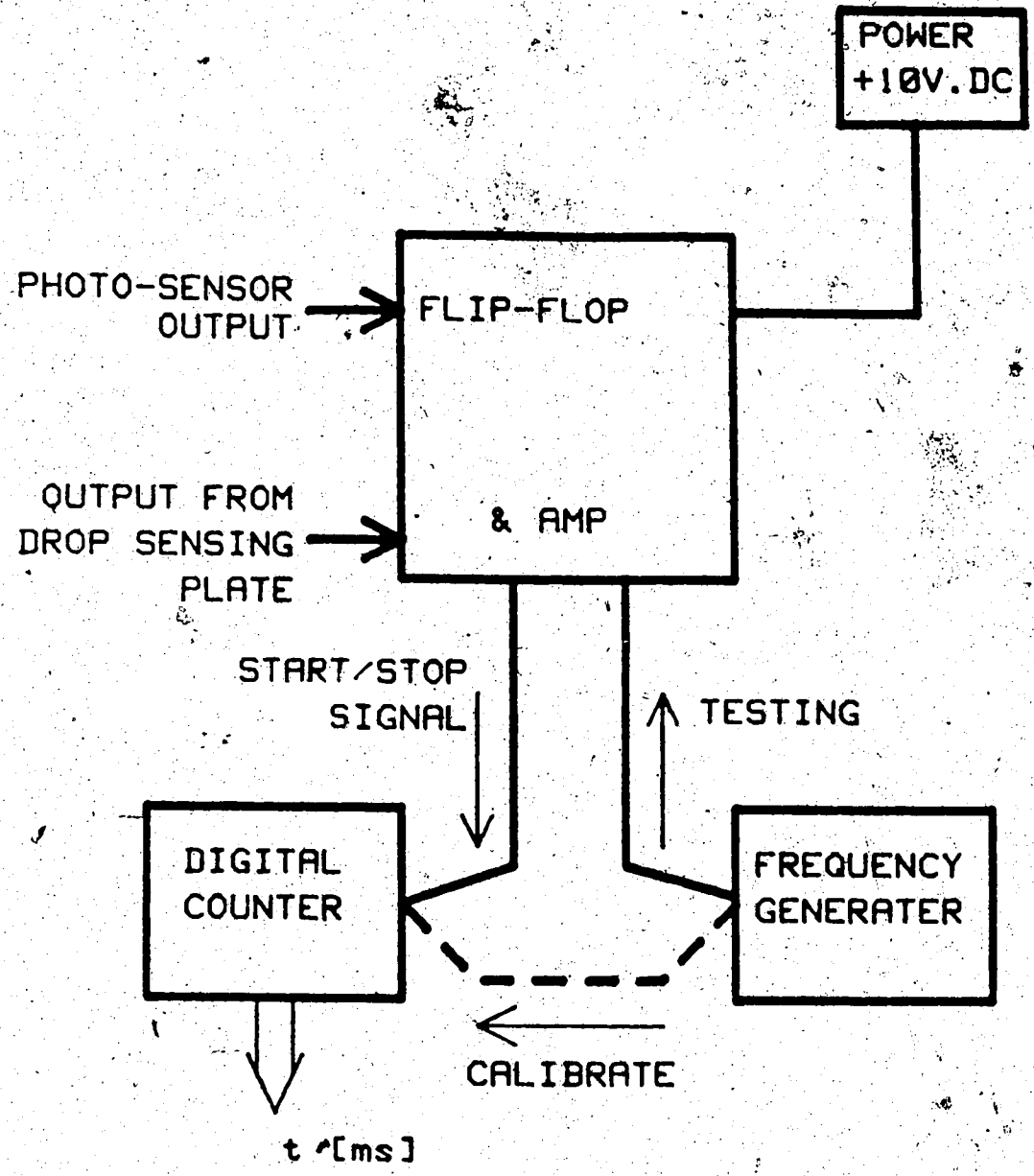
FIGURE 2.7 Drop timing circuit used to determine the time required for the drop to fall the distance H2 as shown in Figure 2.1.

a freely falling water drop (Auld, 1980 and Pruppacher and Klett, 1978). To account for the fact that the drops are moving relative to the air, the drop temperature was calculated simultaneously with its velocity in the iterative "Velocity" program. The appropriate equations and the development of the iterative scheme can be found in Appendix B. Table 2.3 summarizes the drop temperature at impact for 2.4, 2.0, 1.5 and 1.1 mm diameter drops falling in either room temperature (20°C) or -20°C air (the drop temperature was initially 1°C). The table illustrates that none of the drops used in this experimental study would be supercooled (<0°C) at the time of impact.

In order to determine the temperature of the drops at the moment of contact with the impact surfaces, it is required that the drop's initial temperature upon leaving the dropping tip be known. This temperature was obtained by placing a thermocouple inside the reservoir which supplied the drop production water near to the dropping tip, as illustrated in Figure 2.8. The reservoir temperature was held constant by the continuous circulation of a glycol cooling bath.

2.6 Spreading Test Procedures

2.6.1 Photographic Techniques

As stated previously the majority of the experimental

TABLE 2.3   A comparison of the drop temperature at impact
for drops falling in the cold room or in room
temperature air.

Drop Diameter D_d (mm)	Drop Temperature[1] at Impact T_d ($^{\circ}$C)	
	Falling in Cold Room[2] $T_a = -20^{\circ}$C	Falling at room temp. $T_a = 20^{\circ}$C
2.4	1.16	1.30
2.0	1.19	1.42
1.5	1.16	2.16
1.1	0.15	2.94

1   Initial drop temperature = 1°C.

2   Drops fall 0.5 m in room temperature air before
falling an additional 1.185 m in the cold room.
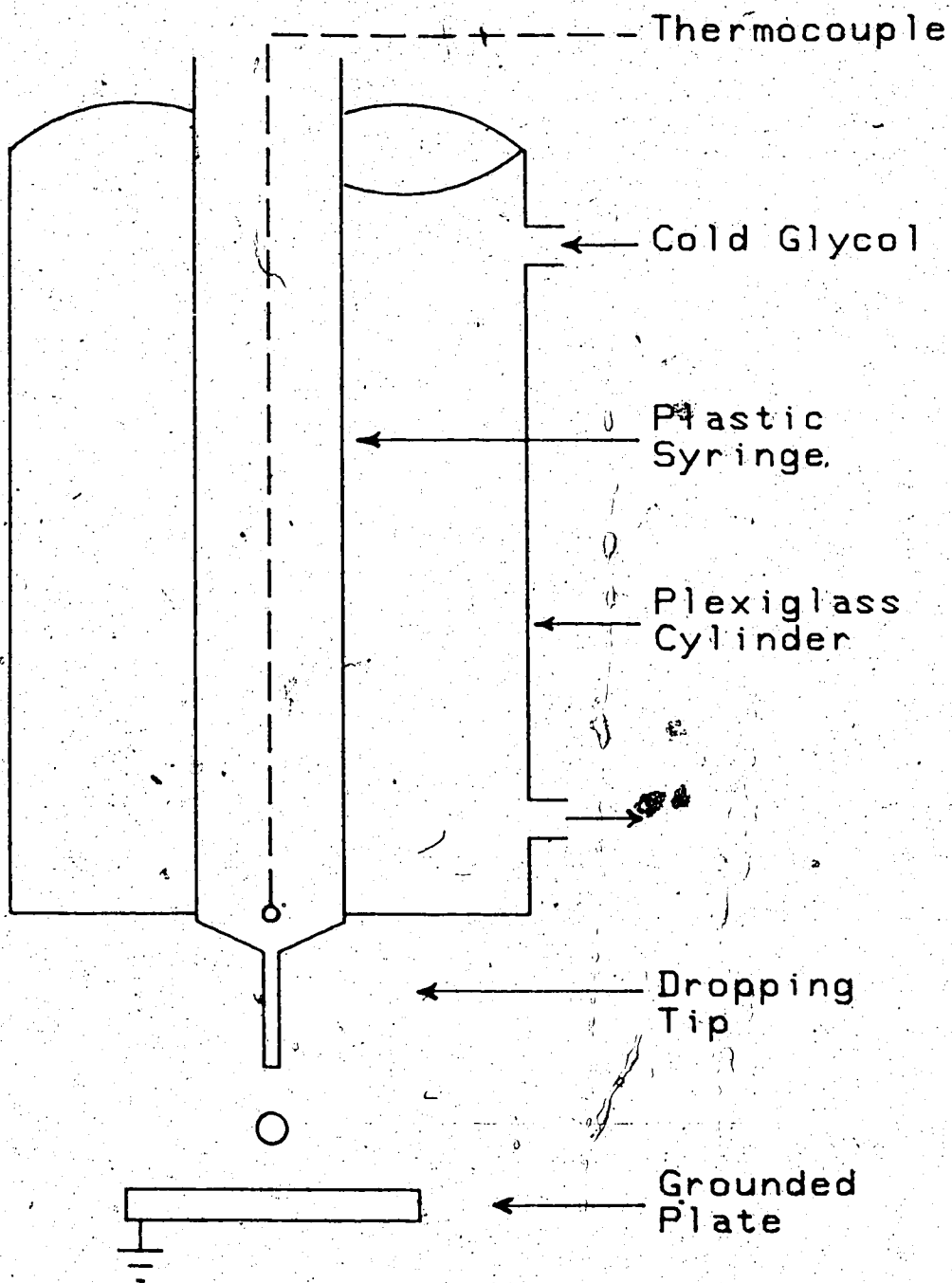
FIGURE 2.8   Schematic of the cooling reservoir used to
control the initial drop temperature.

tests utilized a 35 mm single lens reflex camera to record
the spreading of drop on cold dry surfaces. In order to
produce a "motion picture" like sequence of photographs
(Plate 2.1) required consistently sized drops and a
measurable time delay.

This method was selected over high speed photography
for a number of reasons. One of the major pitfalls of high
speed photography is the possibility that the event may
not be captured on the film. Whether it be lighting or
focus problems or simply the event occurring outside the
field of view of the camera. Needless to say the results
are not known until the film has been developed. Another
problem associated with high speed photography is the
waste of a large portion of the film while the camera
reaches its operating speed.

The basic procedure used in this study was to
photograph a sequence of drops having the same impact
velocity and diameter but at different times during the
spreading process. Note that for each of the times several
photographs were taken to ensure the repeatability of the
results. Figure 2.1 shows a schematic of the set-up used
to photograph the impacting drops. As illustrated in the
figure, a laser beam and a photo detector were placed at a
known distance (H2 = 98.5 cm) above the impact surface.
The photo detector was used to generate an electrical
signal when the drop fell through the beam. The signal was
used in conjunction with the time delay generator to

PLATE 2.1   Sequence of photographs illustrating the
            spreading of a 2.4 mm diameter water drop on
            a -20°C smooth glass plate (V_{im} = 4.8 m/s).
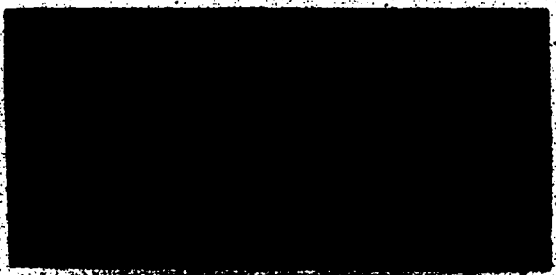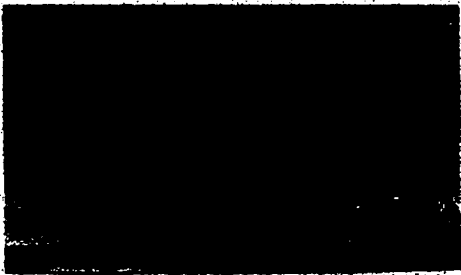
t=time S.F.=swelling factor   t = ...
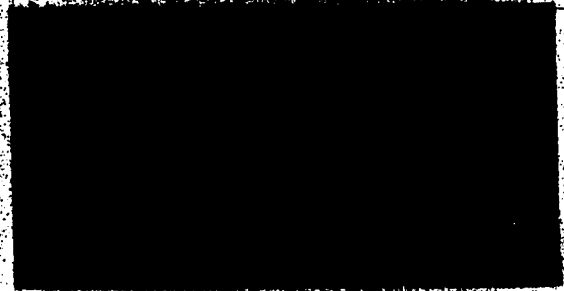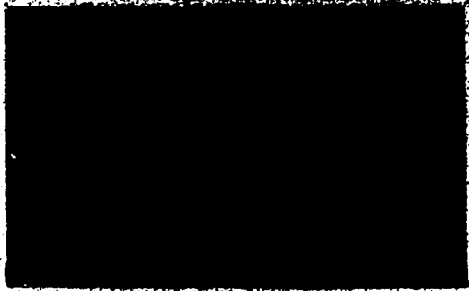
t = 0.15 ms   S.F. = 1.75   t = ...
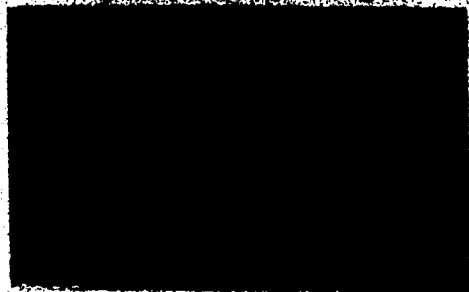
t = 0.3 ms   S.F. = 2.67   t = ...   S.F. = 5.21
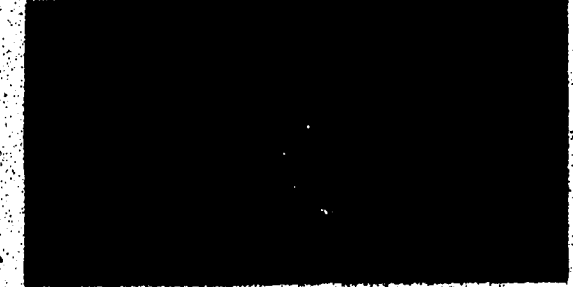
t = 0.5 ms   S.F. = 2.98   t = 6.25 ms   S.F. = 5.08
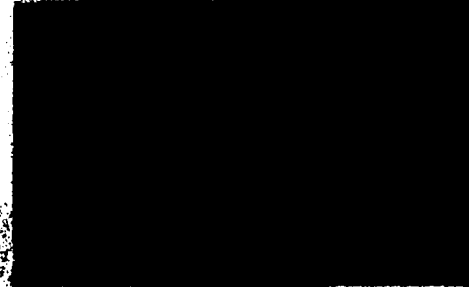
t = 1.0 ms   S.F. = 3.75   t = 9.25 ms   S.F. = 4.88

produce a single short (< 5 μs) duration flash from the strobotac. The time delay generator was capable of delaying the signal (flash) by 1 μs to 100 seconds. For the first drop in the "movie-like" sequence, the appropriate time delay was the time required for the drop to travel the distance H2. Once this time was known, the cold room was darkened, the camera's shutter opened and the motion of the drop was effectively "stopped" by the relatively short flash and captured on the film. The drop was removed from the surface and the procedure was repeated several times.

The subsequent drops were photographed with a correspondingly longer delay time, resulting in the "movie-like sequence (Plate 2.1). This method, although very time consuming, did prove to have certain advantages. The photographs were very detailed and sharp and could be used to obtain the spreading sizes and shapes of the impacting drops, as functions of time. The method also reduced the need to process and sort the huge amounts of film and data that would be produced using a high speed camera.

Dimensional quantities were obtained from the photographs by simply including a scale in the photograph. The photographs were also be used to obtain an independent value of the drop diameter to compare with that calculated from the mass of 100 collected drops. The comparison indicated that the two methods agreed to within

approximately 2% with respect to the drop diameters.

2.6.2 High Speed Video Techniques

Part way through the completion of the experimental portion of this study, the use of a Kodak High Speed Video "Camera" was made available by the Department of Electrical Engineering. The camera is one of only two presently operating in Canada. The camera was capable of framing rates ranging from 60 to 2000 frames/second. In addition, it was possible to produce 6 images per frame thus providing a maximum equivalent framing rate of 12,000 frames/second. This corresponds to 0.083 ms per image making the video ideally suited to record the spreading of the drops considered in this study.

The principle behind the video camera's operation is to record the image using a grid of pixels (i.e. light sensitive diodes). The electronic circuitry converts the image from the diodes into a black and white image recorded on a video tape. The major advantage of the high speed video system is its ability to instantly reproduce the recorded sequence. This ability can be greatly appreciated by anyone who has worked with a high speed camera. Other advantages of the high speed video system are the capability of explicitly displaying the time between frames and the ease at which linear measurements can be obtained from the images.

After recording the sequence of interest the video

tape could be simply rewound and viewed on a video screen, frame by frame (Plate 2.2). In addition to the recorded image, the system overlayed an "informative" frame around the perimeter of the image. The frame provided the framing rate, the time of day and the date, the particular frame number and a test identification number. As mentioned previously, the images are representative of a grid of pixels. As illustrated in Plate 2.3, horizontal and vertical cursors could be superimposed on top of the image. The cursors could be moved manually and their position in terms of pixels displayed in the "informative" frame. The insertion of a scale in the image provides the conversion to actual dimensions. The image on the screen can be transferred to a standard video recorder for future use.

The actual test procedure and equipment was the same as that described in 2.6.1 Photographic Techniques, with the exclusion of the elaborate timing circuits. An additional problem arose since the tests had to be performed in the Electrical Engineering building without the aid of a cold room. To accomplish the freezing of the drops on cold dry surfaces, a portable cooling plate was used. The cooling plate consisted of a copper plate, 6 inches square (15 cm) and 1/8 of an inch (0.3 cm) thick. Soldered to the bottom of the plate was a helically wound coil of 5/16 inch (0.7 cm) copper tubing. The entire plate was enclosed in an insulated box. The cooling was provided
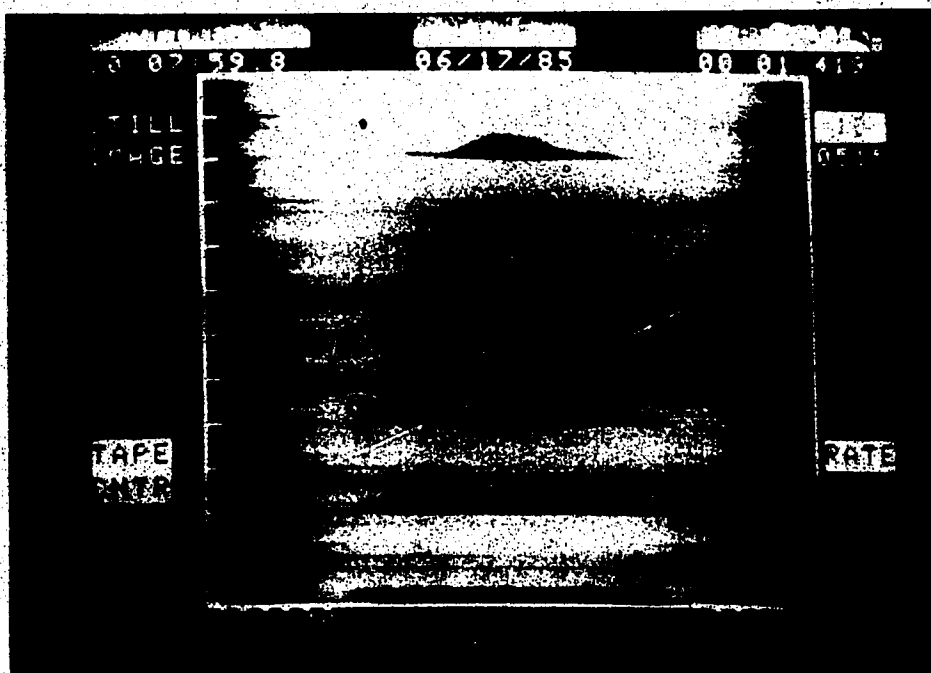
PLATE 2.2 The image produced by the Kodak high speed video system for a 2.4 mm diameter distilled water drop spreading on a -10°C copper plate.
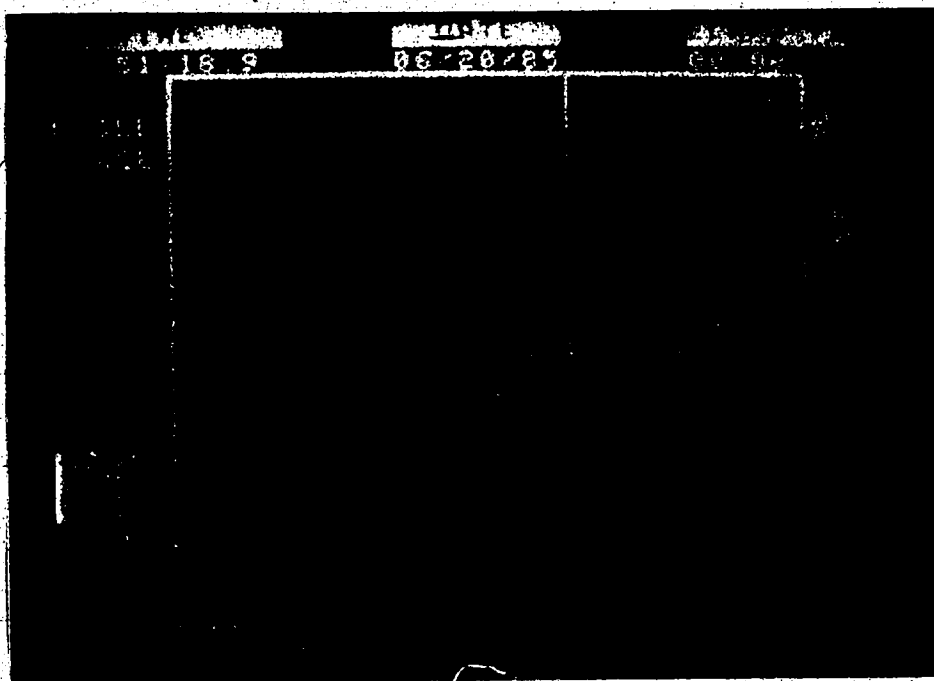
PLATE 2.3 An illustration of the cursors used to measure spreading drop dimensions directly from the Kodak high speed video image.

by circulating glycol from a large temperature-controlled bath. The temperature of the plate was recorded by a surface-mounted thermocouple and the temperature of the bath adjusted accordingly. The actual impact plates were placed directly on top of the cooling plate and allowed to cool to the test temperature.

2.7 FREEZING TIME TEST PROCEDURE

In addition to photographing the spreading of the drops, separate tests were performed to quantify the time required for the single drops to freeze on the cold surfaces. The tests were performed in the cold room utilizing the portable cooling plate because it provided better control of the impact surface temperature. The basic procedure was to allow the single drops to impact, spread and freeze on the impact surface at the location where a thermocouple was mounted flush with the surface.

The surface mounted thermocouple was prepared as follows, to minimize any affect on the spreading process. First a small groove large enough to accommodate a 36 gauge thermocouple wire was machined into the top of the impact surface. Then two holes were drilled perpendicular to the groove through to the bottom of the plate. The copper and constantan wires were inserted through these holes before being butt welded and epoxied into position (i.e. into the groove). The plate was polished using 0.05 μm gamma alumina grit to the surface roughness given

in Section 2.3. This special care was taken to ensure a rapid response time for the thermocouple.

A Hewlett Packard data acquisition unit (Figure 2.9) was used to record the thermocouple output. The data acquisition was limited to readings per second.
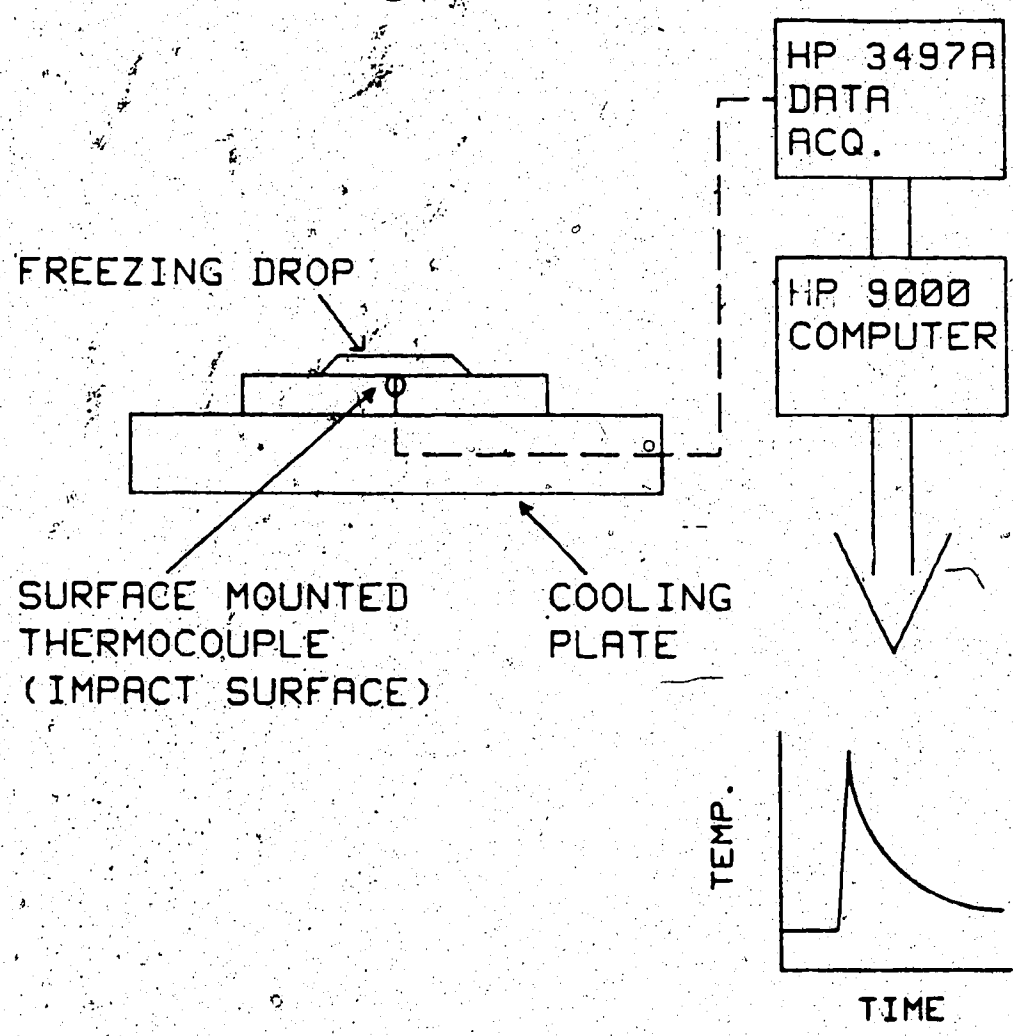
FIGURE 2.9   Schematic of the Hewlett Packard data
acquisition system used in recording the
impact surface temperature during the
freezing of a drop on the surface.

CHAPTER 3

PRESENTATION OF RESULTS

3.1 Introduction

The purpose of the experimental portion of this study was to examine the physical processes that occur during the impacting, spreading and freezing of single drops on cold dry surfaces. These physical processes include the heat flux to the icing surface, the viscous dissipation during spreading, and the effects of the surface tension forces. Of particular interest to the present study was the determination the effects of salinity, drop diameter and velocity, impact surface temperature and roughness on the spreading process. This was accomplished by measuring the size of the spreading drop (i.e. spreading factor Figure 3.1) as a function of time. The ranges of the parameters were chosen to correspond to a "typical" marine icing situation, characterized by large saline drops, that are generally not in thermodynamic or kinematic equilibrium with the surrounding environment (Lozowski and Gates, 1985).

3.2.1 Spreading of Drops on a Warm Surface

Plate 3.1 shows a 2.55 mm distilled water drop impacting with a speed of 4.23 m/s on a smooth glass surface. The sequence of 10 photographs illustrates the spreading of the drop on the glass surface from the time
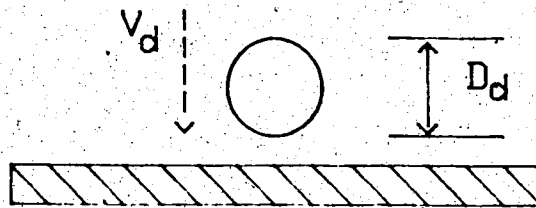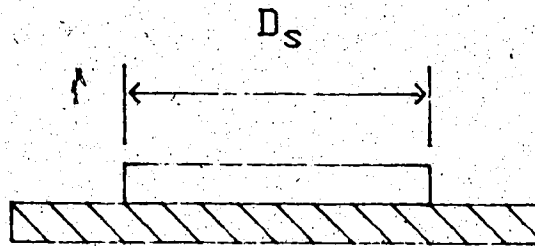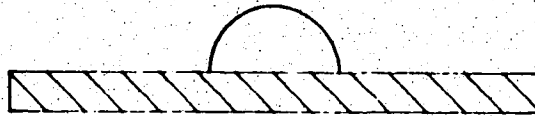
FIGURE 3.1 The definition of Spreading Factor (S.F.)
           as used to specify the size of a spreading
           drop.

PLATE 3.1 Photographic sequence illustrating the
spreading of a 2.55 mm diameter waterdrop on a
room temperature glass surface (V_{im}=4.23 m/s).
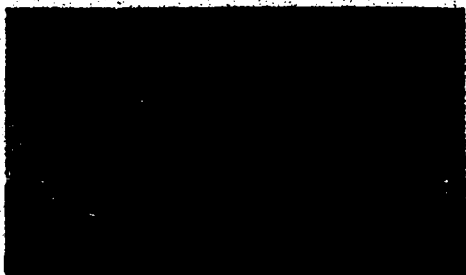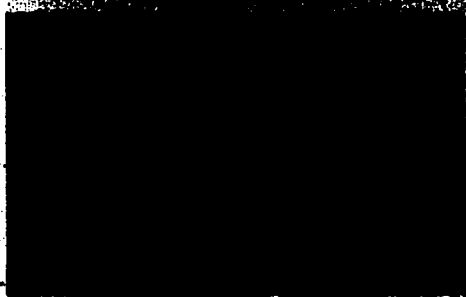
t = 0.75 ms   S.F. = 3.33   t = 3.2 ms   S.F. = 5.33

it impacts until the drop reaches its maximum spread-out size $(S.F._{max})$. Thus plate provides an illustrated perspective of the spreading process on a warm surface for comparison with the spreading and freezing of a drop on a cold surface.

The first photograph in the sequence shows the initially spherical drop an instant ($\approx.1$ ms) before it impacts on the surface. Just after the drop impacts it remains essentially spherical with the exception of a small portion in contact with the surface. Even at this initial stage of the spreading the drop has begun to spread radially outward, from the point of impact on the surface. This is illustrated by the thin "band" or "ring" of water with a circumference slightly larger than the circumference of the section of the drop in contact with the surface, as visible in the 2nd photograph in the sequence. As the apex of the drop moves closer to the impact surface, the drop begins to flatten and deform as the circumferential "ring" enlarges (3rd photograph in the sequence). At this point there is a smooth transition between the remaining portion of the drop (i.e. remaining portion of the initially spherical drop) and the circumferential "ring".

The apex of the drop continues to move toward the surface while mass from the drop "flows" into the "ring" increasing it's circumference. As the spreading continues the leading edge of the "ring" begins to thicken as

illustrated in the 5th photograph in the sequence. This thickening of the leading edge becomes well-defined by the time the apex of the drop has completely dissappeared (7th photograph). At this point, the initially spherical "drop" is comprised of what appears to be a "disk" of water with a somewhat thicker and bumpier circumferential "ring".

The "disk" continues to increase in diameter while the leading edge (ring) thickens and the bumps or ripples become more evident (8th and 9th photographs in the sequence). This ripply or wavy appearance of the leading edge corresponds to the formation of a gravity wave. The disk continues to spread until it reaches its maximum spread out size referred to as $S.F._{max}$. As illustrated in the 10th photograph in the sequence where the drop has reached $S.F._{max}$, the gravity wave is now well defined in the relatively thick leading edge of the spread-out drop.

The shape of the spread-out drop illustrated in the 10th photograph of the sequence does not represent the final shape of the drop on a warm surface. As a result of being "spread out" on the surface, the surface tension forces cause the drop to "contract" and take on the shape of a somewhat flattened "hemisphere" of water, with a diameter of approximately twice its initial spherical diameter. This final shape is obtained when the gravitional potential and surface tension forces are in equilibrium. The above description only holds true if the

water "wets" the surface, (i.e. the contact angle is less than 90°), as is the case with water on glass.

3.2.2 Spreading of Drops on a Cold Surface

For comparison with the spreading of a drop on a warm surface, Plate 3.2 shows the spreading of a 2.55 mm diameter distilled water drop on a -10°C glass surface. The drop arrived at the surface with an impact velocity of 4.23 m/s and a temperature of 1°C. With the exception of the -10°C glass surface the conditions under which the spreading occurs are identical to those used to illustrate the spreading of a drop on a warm surface (Plate 3.1). A comparison of these plates illustrates two of the obvious affects that freezing (heat transfer) has on the spreading process.

On the warm surface, after the apex of the drop is no longer apparent (7th photograph, Plate 3.1), the "ring" of water at the leading edge of the spreading drop begins to form a gravity wave. This gravity wave is well defined by the time the drop reaches S.F.$_{max}$ (10th photograph, Plate 3.1). However on the cold surface, although there are indications that the gravity wave is beginning to develop (7th photograph, Plate 3.2), by the time the drop reaches S.F.$_{max}$ the gravity wave is no longer apparent (9th photograph, Plate 3.2).

The second effect of the freezing (i.e. heat transfer) on the spreading process is obvious from the 10th
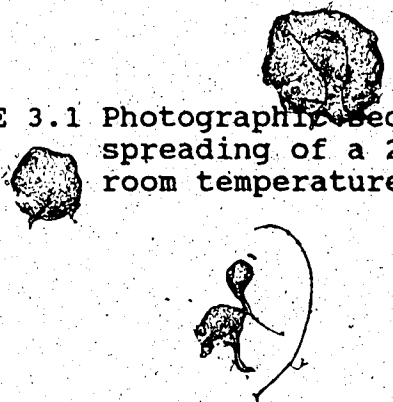
PLATE 3.2 Photographic sequence illustrating the
spreading of a 2.55 mm diameter waterdrop
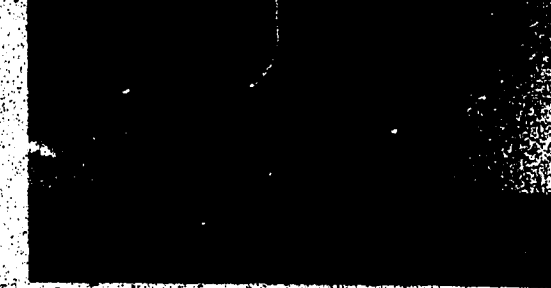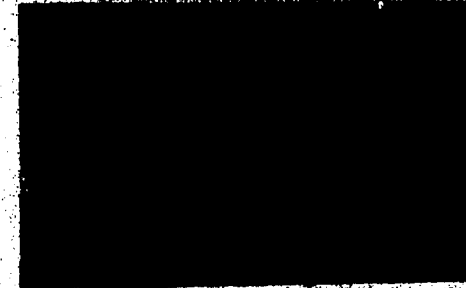on a -10°C glass surface ($V_{im} = 4.23$ m/s).
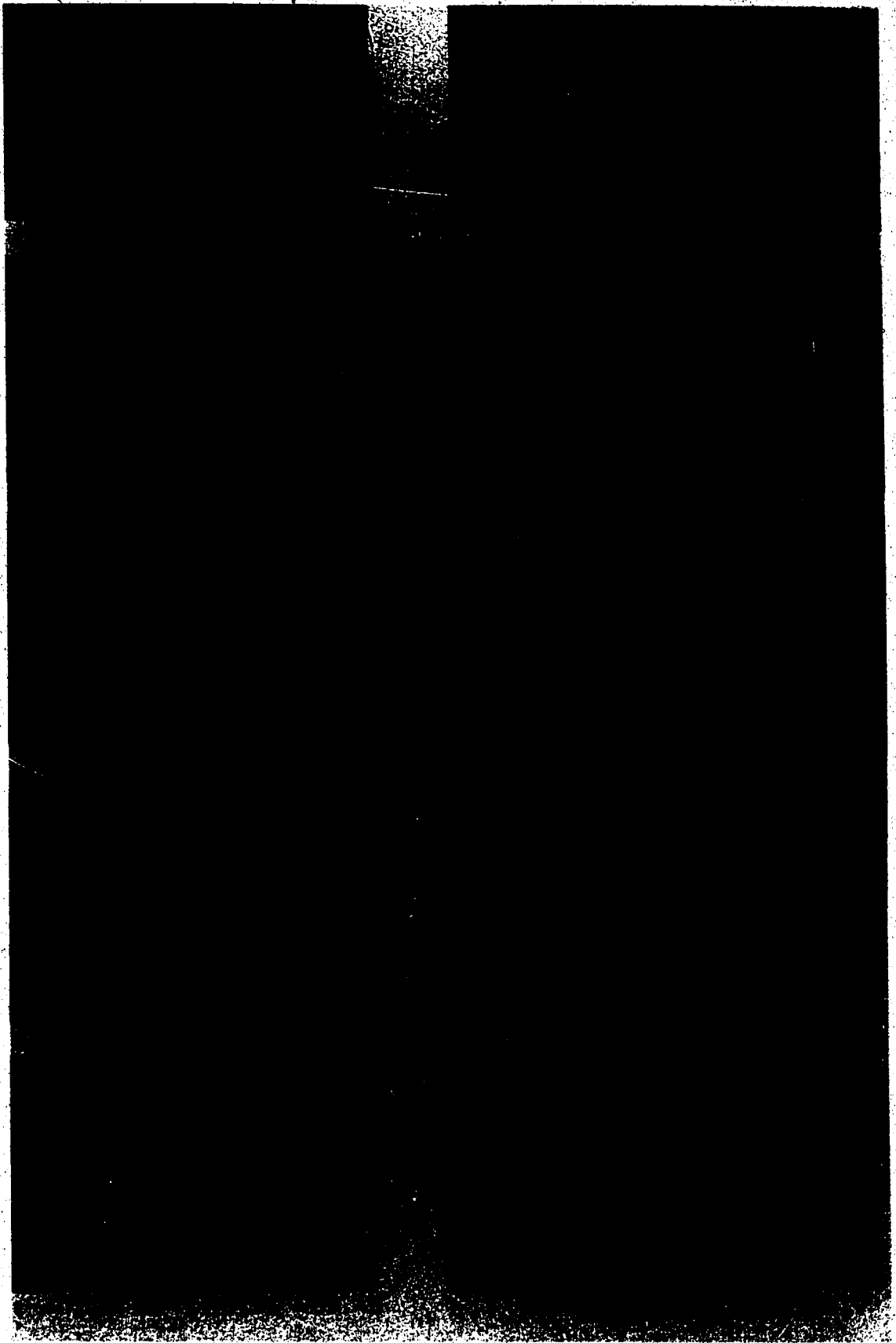
photograph in Plate 3.2. This photograph shows the final shape of the drop as a relatively flat layer of ice, in comparison with a drop on a warm surface where the equilibrium (i.e. final) shape has a somewhat "hemispherical" profile. However, it is the large difference in the final spread out size (S.F.) which is of particular importance. It is also interesting to note that for the drop spreading on the cold surface the width of the "ring" at the leading edge of the spreading drop is larger for the equilibrium shape (10th photograph) than for the shape corresponding to S.F.$_{max}$ (9th photograph, Plate 3.2). This gives the frozen drop a flat "donut" like appearance (i.e. a depression in the central portion of the spread out drop).

Plates 3.3 and 3.4 show the final size and shape of 2.4 mm drops frozen on -20°C copper and ice surfaces after impacting on the surfaces at 4.8 m/s. Both Plates indicate the depression in the center of the "donut" like shape; however, the diameter of the depression is smaller for the ice surface.

3.3 Spreading Results

3.3.1 Spreading Factor verses Time

For illustrative purposes Figure 3.2 plots the spreading factor of drops spreading on a warm (>20°C) copper surface, as a function of time, for Impact Weber
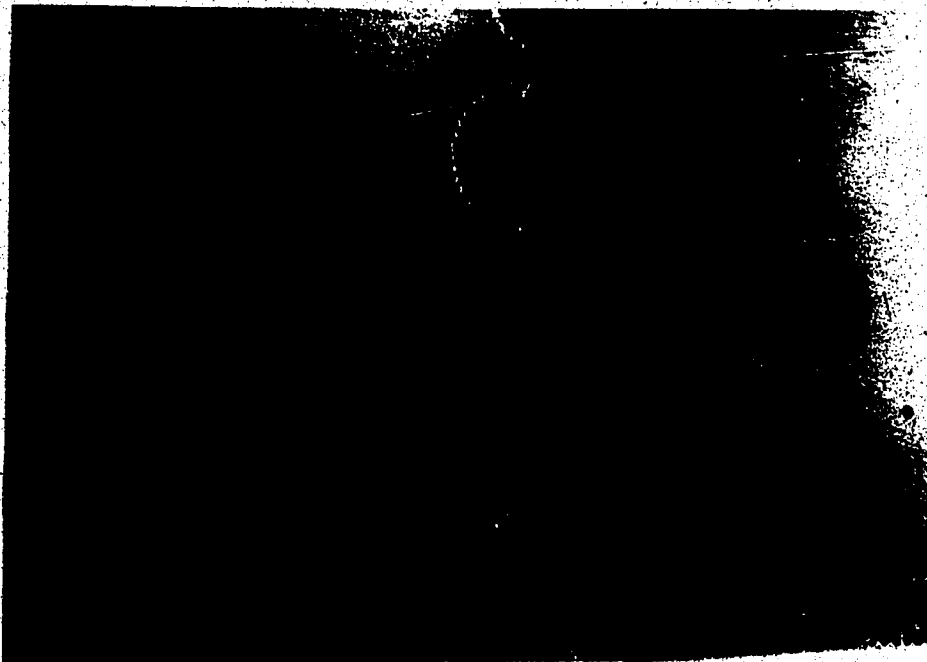
PLATE 3.3 Final size and shape of 2.4 mm diameter
salt water drops freezing on a -20°C
copper surface (V$_{im}$ = 4.8 m/s).

PLATE 3.4 Final size and shape of 2.4 mm diameter drops
freezing on a -20°C ice surface (V$_{im}$=4.8 m/s).
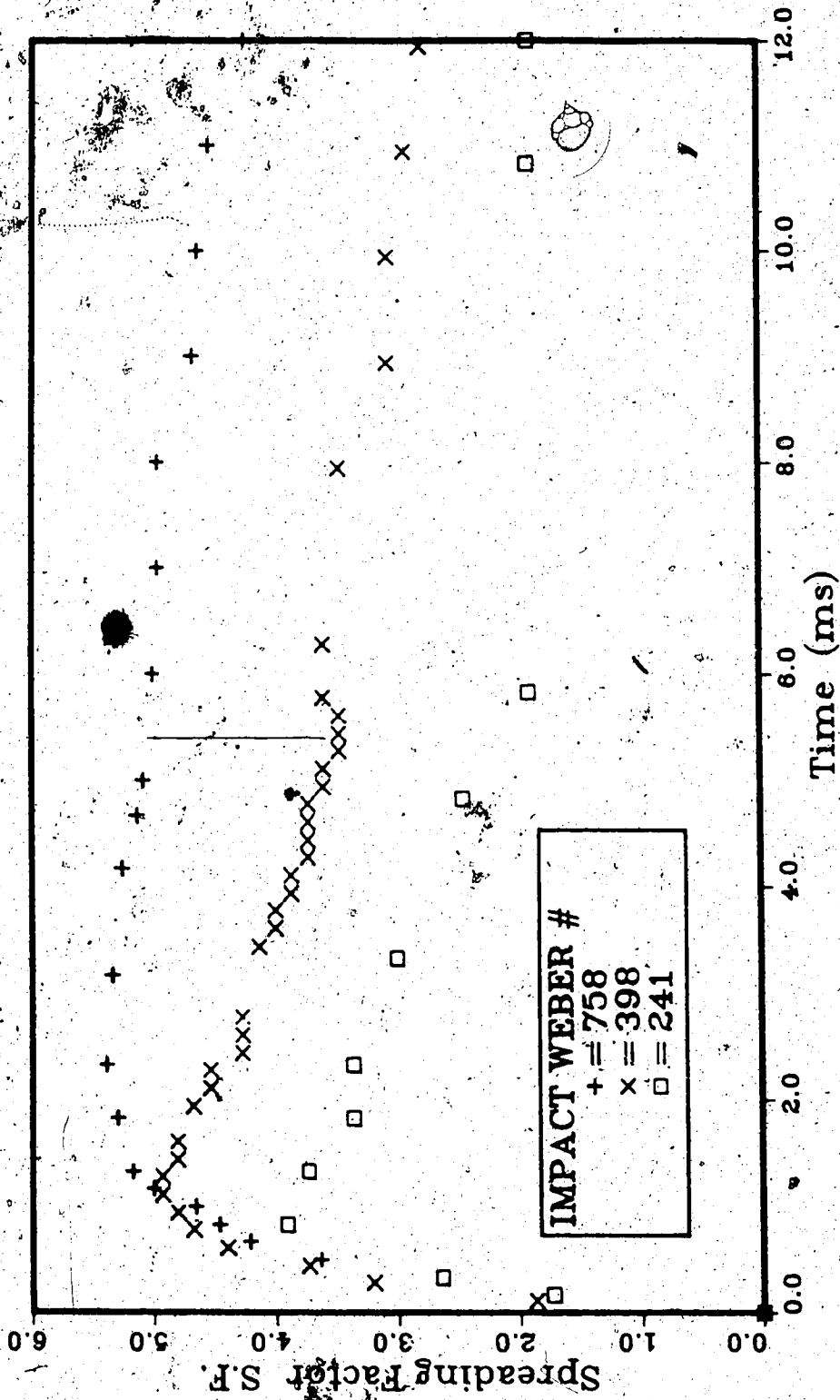
FIGURE 3.2   The spreading factor of distilled water drops spreading on a warm (20°C) copper surface.

Numbers of 758, 398 and 241. The Impact Weber Number (We #) is defined as 12 times the ratio of the kinetic to surface energy of the impacting drop and is given by:

$$We \# = \rho_w V_{im}^2 D_d / \gamma_{a/w} \qquad (3.1)$$

where

$\gamma_{a/w}$ = surface tension coefficient for air-water interface

= 73 dyne/cm = .073 nt/m

The Impact Weber Numbers of 758, 398 and 241 referred to in Figure 3.2 represent 2.4, 1.5 and 1.1 mm diameter distilled water drops impacting at 4.8, 4.4 and 4.0 m/s respectively. A simple dimensional analysis suggests that the spreading factor (D_s/D_d) is a function of the Reynolds number and Weber number. Since the Weber number represents the two most important components of the drop energy, namely the kinetic and surface energy, which are of particular importance especially during the initial stages of spreading, the Impact Weber number was choosen to nondimensionalize the impacting drop parameters. In addition, due to limitations of the experimental set-up the drop velocities were not varied independently of the drop diameters. The Weber number conveniently allowed the drop diameter and the corresponding velocity to be represented by a single non-dimensional variable.

Figures 3.3 and 3.4 are also plots of the spreading factor as a function of time, except that the spreading is
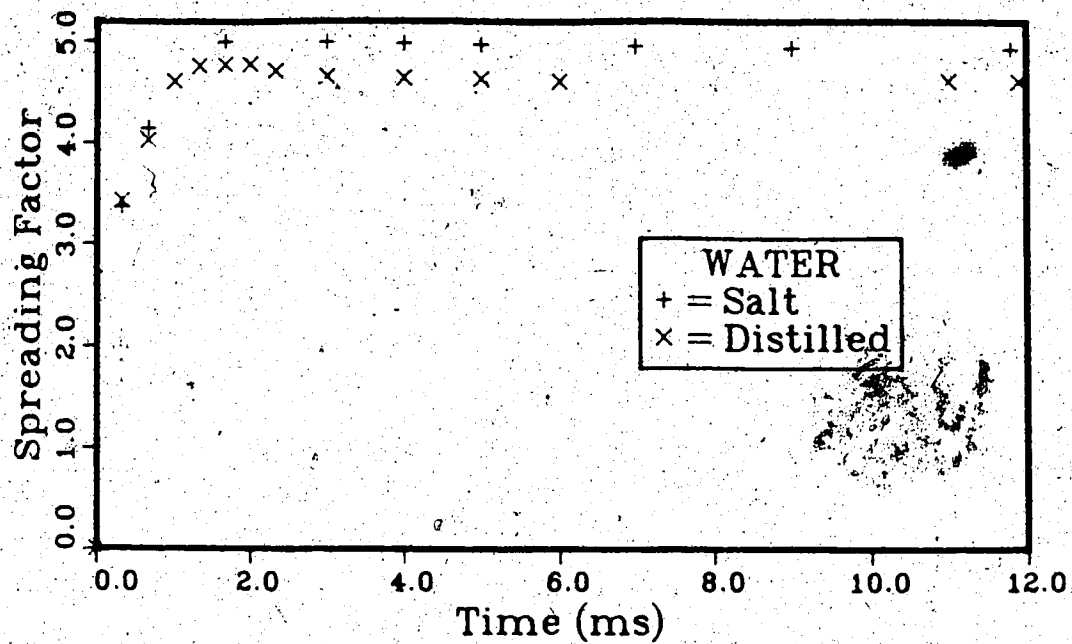
FIGURE 3.3   The effect of salinity on the spreading of
             2.4 mm diameter waterdrops on a -20°C copper
             surface (V_{im} = 4.8 m/s).
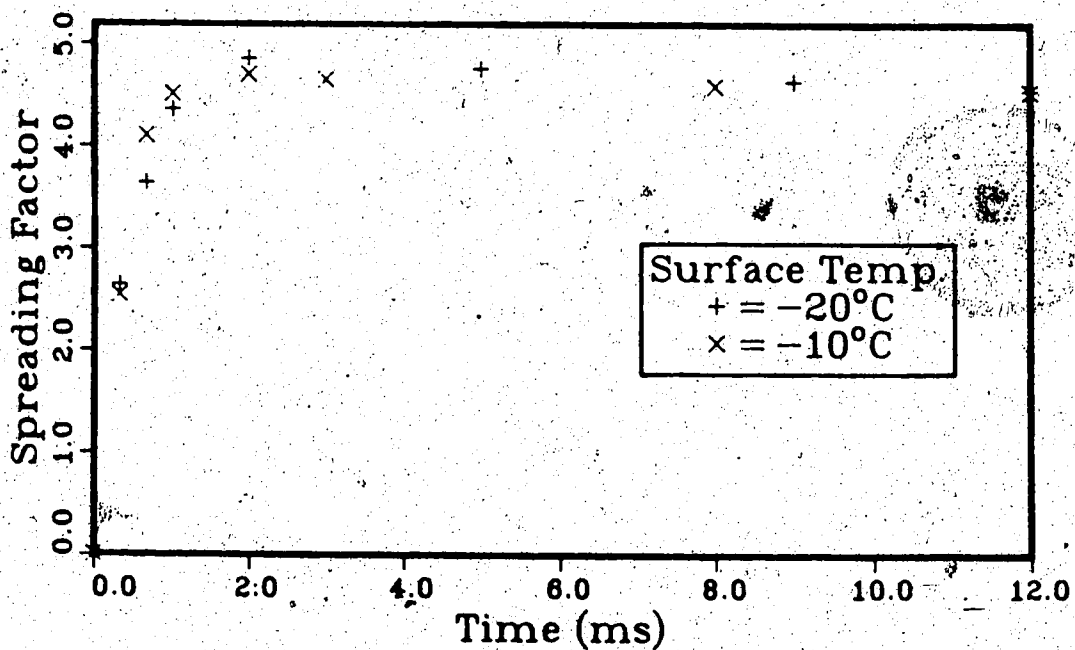
FIGURE 3.4   The effect of impact surface temperature on
             the spreading of 2.4 mm diameter waterdrops
             on a stainless steel surface (V_{im}=4.8 m/s).

occurring on a cold surface. Figure 3.3 shows the effect of salinity on spreading of a 2.4 mm drop (V_{im} = 4.8 m/s) on a smooth -20°C copper surface, while Figure 3.4 shows the effect of the impact surface temperature (-10, -20°C) on the spreading of 2.4 mm diameter water drops on a cold stainless steel surface (V_{im} = 4.8 m/s).

3.3.2 Spreading Factor - Maximum

Table 3.1 summarizes S.F.$_{max}$ and the time required to reach S.F.$_{max}$ for drops spreading and freezing on copper, stainless steel and ice surfaces. The table shows the effect of the impact surface temperature (20, -10 and -20°C), We # (241, 398 and 751) and salinity (S=33 g/kg) on S.F.$_{max}$ and the time to S.F.$_{max}$. The values in this table were summarized from a single video or photographic test and due to time limitations were not repeated.

3.3.3 Spreading Speed - Initial

The initial spreading speed (V_s) or radial spreading velocity was said to be the average radial spreading speed from the time of impact until the time t_s, where t_s is equal to D_d/V_{im}, the time required for the impacting drop to move the distance equal to its initial (spherical) diameter. Had the drop's motion not been impeded by the impact with the solid surface, t_s would correspond to the time at which the apex of the impacting drop would no longer be apparent (Plate 3.1, 7th photograph in sequence).

TABLE 3.1 Effect of impact surface temperature and salinity on the maximum spreading Factor (S.F.max) and the corresponding time required to reach S.F.max.

SURFACE		DROP		S.F.$_{max}$		Time to S.F.$_{max}$	
Material	Temp. (°C)	Diameter (mm)	Impact Velocity (m/s)	Distilled	salt	Distilled (ms)	salt (ms)
Copper	20	2.4	4.8	5.38	5.38	2.33	2.33
	-10	2.4	4.8	4.85	5.13	2.00	2.00
	-20	2.4	4.8	4.76	5.00	1.33	1.67
	20	1.5	4.4	4.93	4.93	1.20	1.20
	-10	1.5	4.4	4.85	4.69	1.33	1.00
	-20	1.5	4.4	4.12	4.57	0.91	1.00
	20	1.1	4.0	3.91	3.91	0.83	0.83
	-10	1.1	4.0	3.80	—	1.50	—
S.S. 304	-10	2.4	4.8	4.85	4.86	1.55	2.00
	-20	2.4	4.8	4.31	4.86	1.33	2.00
	-10	1.5	4.4	4.49	4.42	1.17	2.00
	-20	1.5	4.4	4.37	4.11	1.16	1.17
Ice	-10	2.4	4.8	5.00	5.40	2.33	2.44
	-20	2.4	4.8	5.15	5.60	1.67	2.33

Table 3.2 summarizes the effect of salinity and impact surface temperature on the initial spreading rate of the drops. The surface temperatures used for these tests were 20, -10 and -20°C for the copper plates and -10 and -20°C for the stainless steel plates. The effect of We # (241, 378 and 751) on this spreading rate is also illustrated in this table..

3.3.4 Spreading Factor - Final Size

Figures 3.5 through 3.7 show the final size, in terms of spreading factor, as a function of the Impact Weber number (non-dimensional ratio of inertial to surface tension forces). Final size refers to the spreading factor after the spreading and/or freezing have been completed (i.e. equilibrium shape and size). The figures show S.F.$_{final}$ for variations in surface temperature and salinity (S =0 or 33 g/kg) for the drops spreading and freezing on ice, copper and stainless steel surfaces.

Figure 3.5 shows the variation in final size for impact surface temperatures of -10 and -20°C, as well as the effect of salinity for drops spreading and freezing on an ice layer. Figures 3.6 and 3.7 show the variation in S.F.$_{final}$ under the same conditions, except the drops are frozen on copper and stainless steel surfaces. In Figures 3.5 through 3.7 the air temperature was the same as the impact surface temperature and the drops arrived at the

TABLE 3.2 The effect of salinity and impact surface temperature on the initial spreading rate* of water drops on cold dry surfaces (* - average rate until time $t = D_d/V_{im}$).

SURFACE		DROP		Initial Spreading rate/ Impact Velocity	
Material	Temp. (°C)	Diameter (mm)	Impact Velocity (m/s)	Distilled	Salt
Copper	20	2.4	4.8	1.81	—
	20	1.5	4.4	1.71	—
	20	1.1	4.0	1.16	—
	-10	2.4	4.8	1.78	1.77
	-10	1.5	4.4	1.22	1.70
	-10	1.1	4.0	0.89	—
	-20	2.4	4.8	1.86	1.87
	-20	1.5	4.4	1.19	1.47
S.S. 304	-10	2.4	4.8	1.75	1.66
	-20	2.4	4.8	1.65	1.57
	-20	1.5	4.4	1.46	1.71
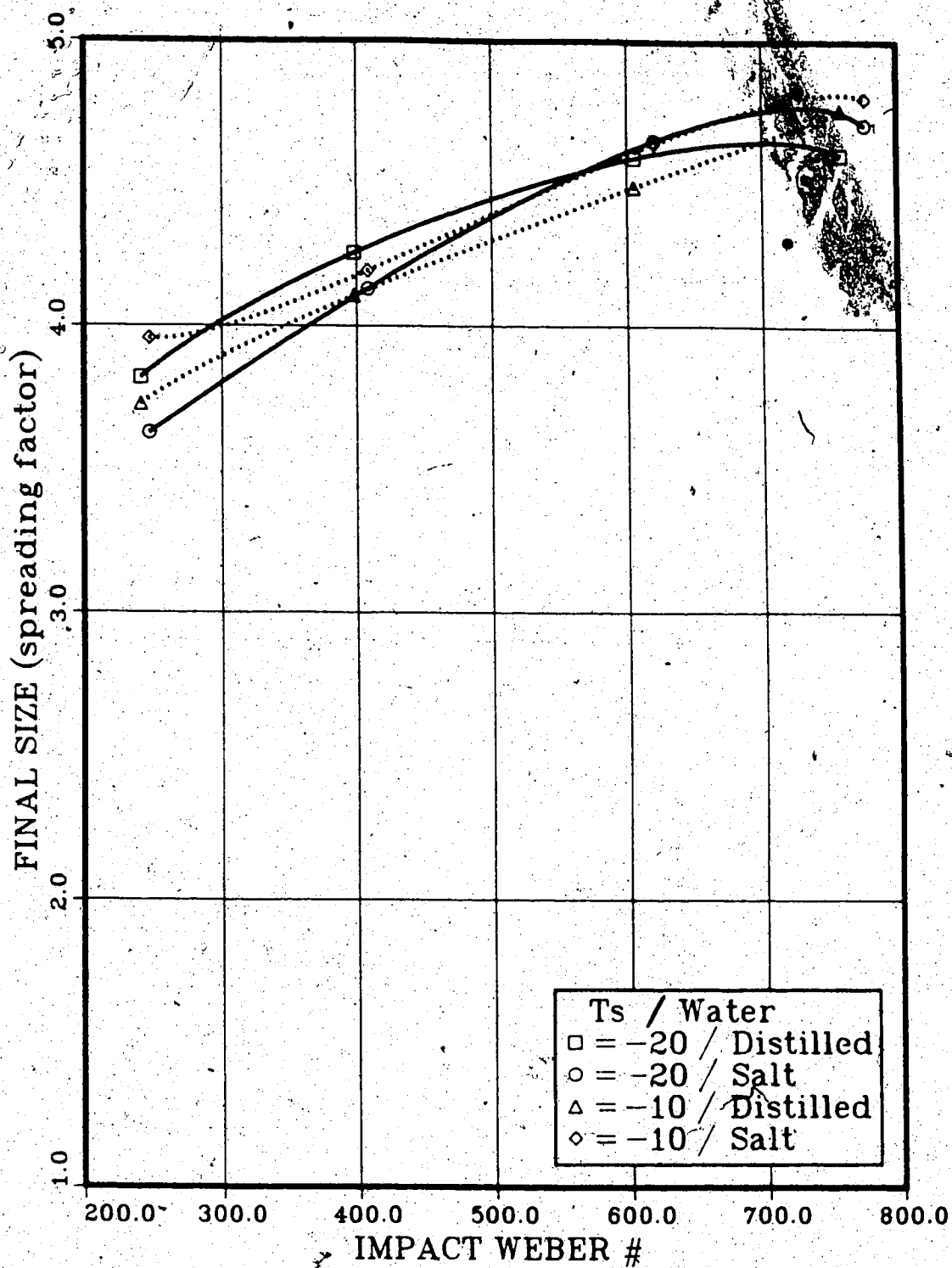
FIGURE 3.5   Final size (S.F.) verses Impact Weber # for distilled and salt waterdrops spreading on -20 and -10°C ice surfaces ($T_{air}=T_s$=temp. of ice surface and $T_{drop}=1°C$).
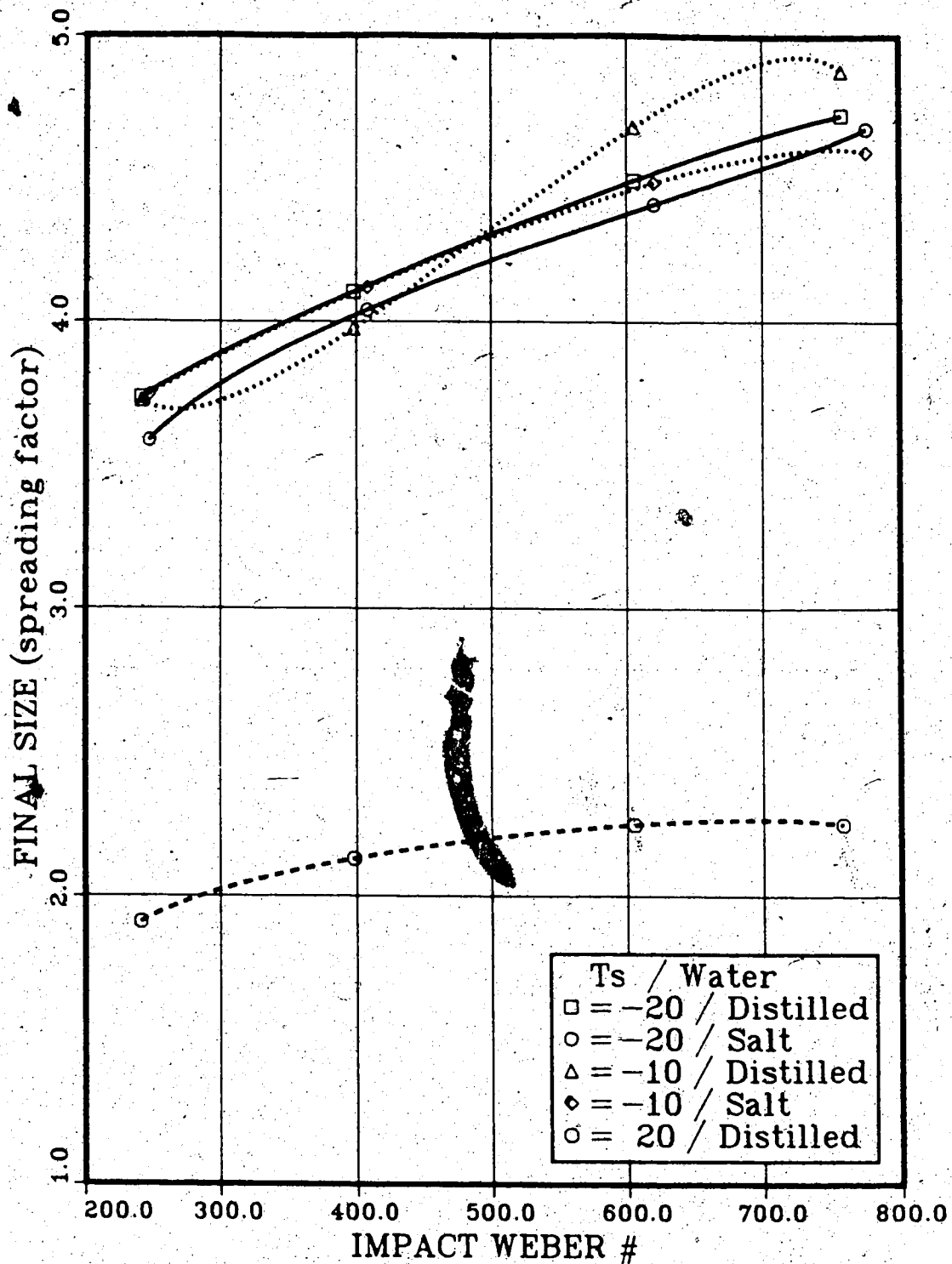
FIGURE 3.6 Final size (S.F.) verses Impact Weber # for
distilled and salt waterdrops spreading on
20, -10 and -20°C copper surfaces ($T_{air}=T_s=$
temp. of copper surface and $T_{drop}=1°C$).
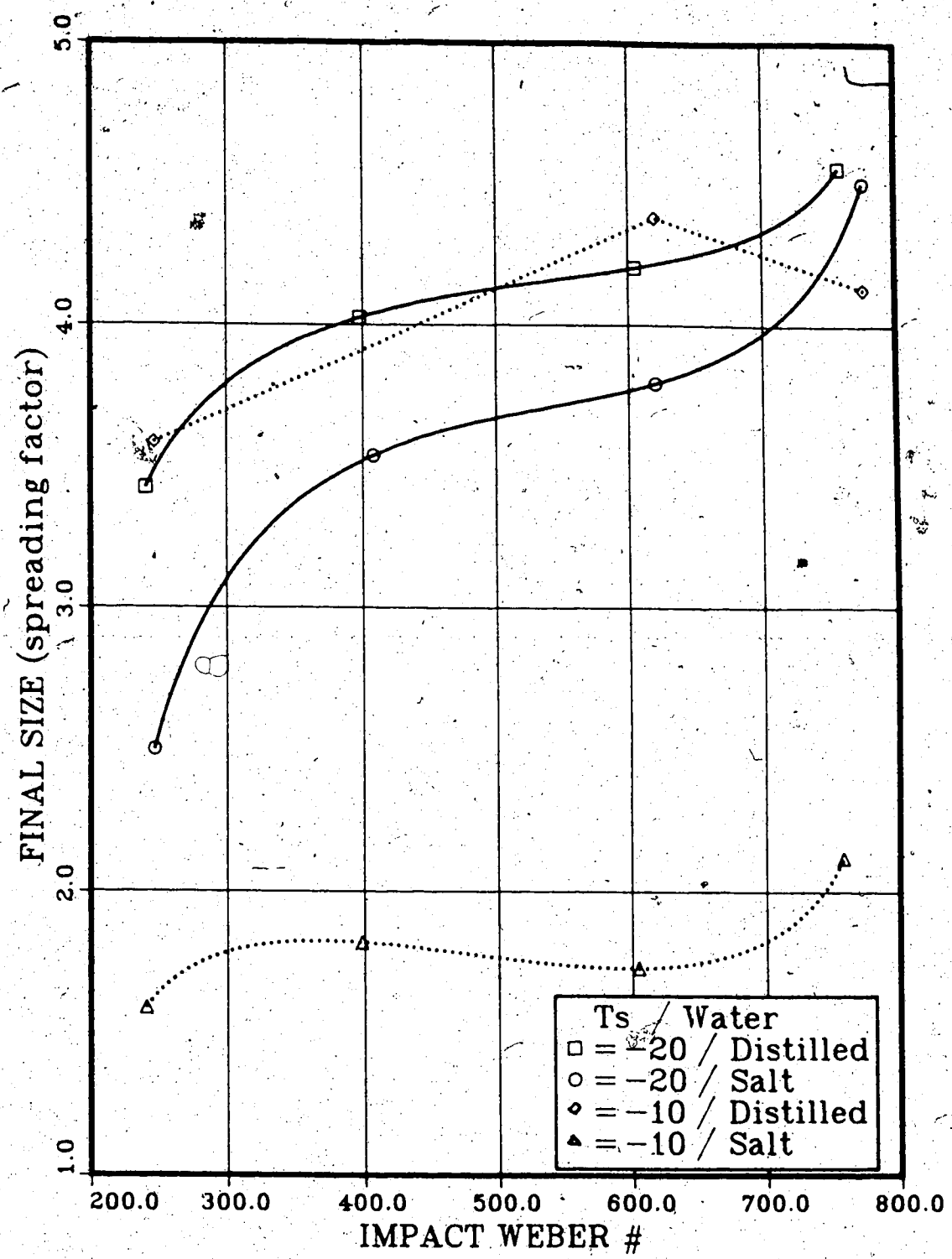
FIGURE 3.7 Final size (S.F.) verses Impact Weber # for distilled and salt waterdrops spreading on -20 and -10°C stainless steel 304 surfaces ($T_{air}=T_s$= temp. of surface and $T_{drop}=1°C$).

surface with a temperature of approximately 1°C.

Note that the experimental tests used to determine the final size of the spread-out drops (i.e. S.F.$_{final}$) were performed independently of the high speed video and photographic sequences. Since only a single photograph of the drops was required to determine the final size, several tests could be performed to insure the results were statistically valid.

3.4 Freezing and Cooling

In addition to determining the size of the spread-out drops, it is important in terms of modelling ice accretions to determine the temperature of the freezing drops as a function of time. Since it was not possible to measure the drop temperature, the impact surface temperature was measured and correlated to the drop temperature.

3.4.1 Freezing and Cooling Times

Figure 3.8 plots the surface temperature of a plexiglass plate as a function of time, recorded during the spreading of a 2.55 mm diameter distilled water drop on the plate. The drop arrived at the surface with an impact speed of 4.3 m/s and a temperature of 4°C and froze as a "disk" of water with a spreading factor of 4.5. The initial surface temperature was -10°C and the air temperature was maintained at -12°C. The figure
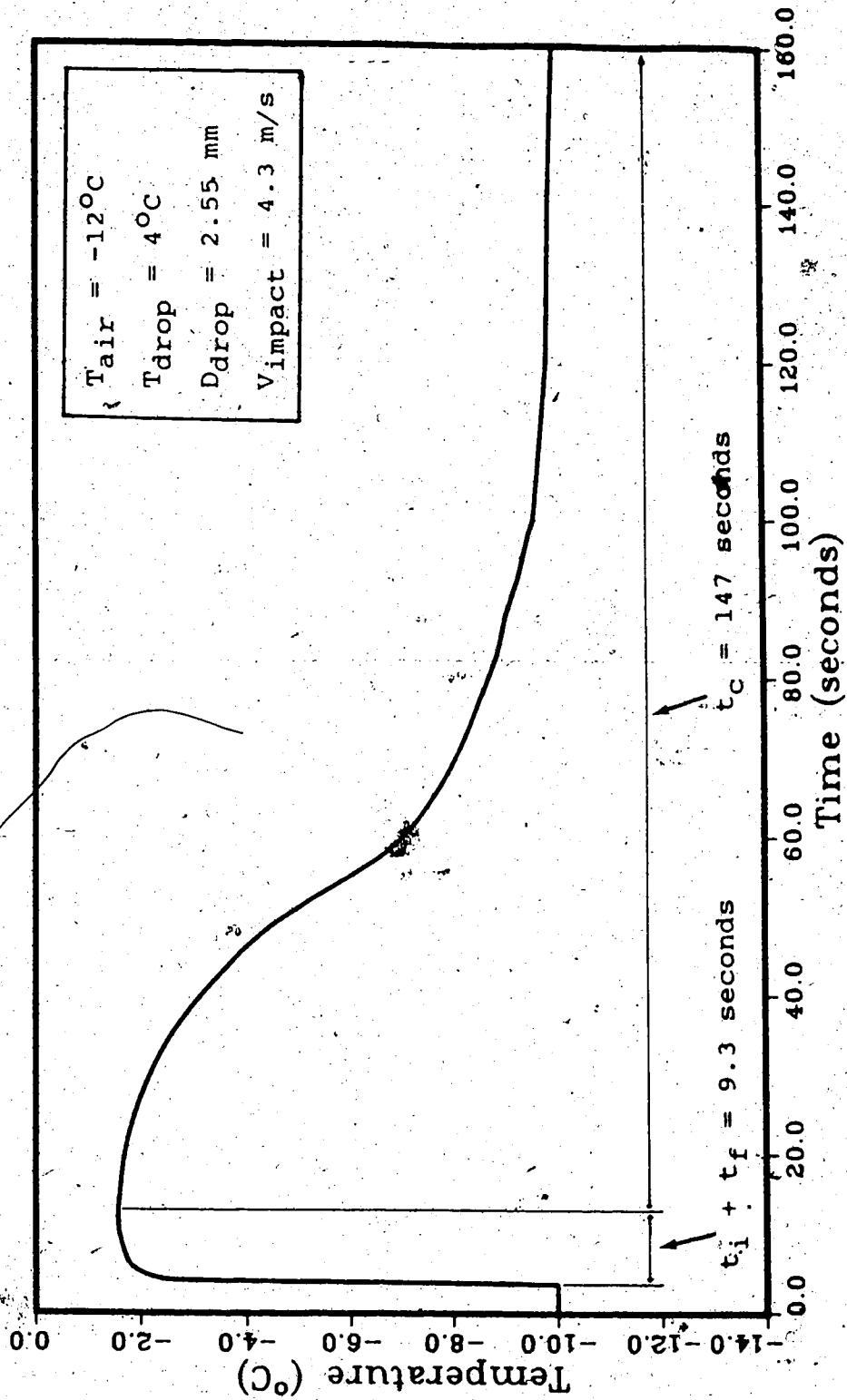
FIGURE 3.8   Freezing of a spread out (S.R. = 4.5) fresh water drop on a
-10°C plexiglass plate. Temperature recorded from a surface
mounted thermocouple.

illustrates the three time periods or stages appropriate to the freezing of the drop and the cooling of the drop and the surface to the initial surface temperature (i.e. temperature of surface prior to the arrival of the drop).

It is the sum of these three times (t_i, t_f and t_c) which is referred to as the total time. The time t_i was equal to zero in this particular case since the impacting drop was not supercooled. This time t_i corresponds to the time required for ice to grow in a "portion" of the drop if the drop is supercooled. This "portion" of the drop is equal to the degree of supercooling times the drop's specific heat capacity divided by the latent heat of fusion. The time t_f corresponds to the time required to freeze the drop (i.e. cool the drop to 0°C and remove the latent of fusion). The time t_c corresponds to the time required to return the impact surface and the drop to the initial temperature of the surface.

Table 3.3 summarizes the experimentally determined freezing times for single distilled and saline water drops freezing on -10 and -20°C copper and stainless steel surfaces. The table includes the freezing times for 2.4, 1.5 and 1.1 mm drops impacting with velocities of 4.8, 4.4 and 4.0 m/s respectively. These times were estimated from the high speed video results by assuming that the drop was frozen when the spreading factor did not change (i.e. time corresponding to S.F.$_{final}$). Since the drops arrived at the surface at approximately 1°C, t_i was taken to be equal

TABLE 3.3 Experimentally determined freezing times for salt and distilled waterdrops on cold dry surfaces ($T_{air} = T_s$ = temp. of surface).

SURFACE		DROP		FREEZING TIME t_f (ms)	
Material	Temp. ($^{\circ}$C)	Diameter (mm)	Impact Velocity (m/s)	Distilled	Salt
Copper	-10	2.4	4.8	16.0	14.0
	-10	1.5	4.4	8.0	6.0
	-20	2.4	4.8	14.0	13.0
	-20	1.5	4.4	6.0	4.0
S.S. 304	-10	2.4	4.8	17.0	13.0
	-10	1.5	4.4	13.0	11.0
	-20	2.4	4.8	10.0	12.0
	-20	1.5	4.4	6.0	6.0
Plexiglass	-10	2.55	4.23	9300	——

to zero.

3.4.2 Total Time

Table 3.4 summmarizes the experimentally determined total time ($t_i + t_f + t_c$) measured using a surface mounted thermocouple and the H.P. data acquisition unit (Section 2.6). The table includes the total time for 2.4 mm drops impacting at 4.8 m/s on -20°C copper and stainless steel surfaces. The table also includes the effect of salinity and the initial drop temperature on t_T.

TABLE 3.4. Total time, t_T ($t_i + t_f + t_c$) required to freeze 2.4 mm diameter waterdrops, impacting at 4.8 m/s, then cool the impact surface to its initial temperature (i.e. t_c = time required to cool impact surface to 99% of $T_m - T_s$).

SURFACE Material	Initial Temp-T_s (°C)	Drop Temp. at Impact (°C)	Salt or Distilled Waterdrop	Total time t_T (ms)	Standard Deviation σ	Sample Size N
Copper	-20	1	d	1730	—	1
	-20	1	s	1890	150	7
	-20	20	d	1900	100	4
	-20	20	s	1990	30	2
S.S.304	-20	1	d	1840	90	3
	-20	1	s	1900	190	2
	-20	20	d	1890	130	2
	-20	20	s	2110	130	3

CHAPTER 4

DISCUSSION OF RESULTS

As a result of the increased activity in offshore operations in northern waters, there has been increased emphasis placed on marine icing research. Of particular interest is the development of analytical models which can be used to predict ice accretion rates and possibly shapes, under typical marine icing conditions. Typical marine icing conditions are characterized by large saline drops which are generally in neither kinematic nor thermodynamic equilibrium with the air (Lozowski and Gates, 1985). The primary source of these drops is the sea spray generated by impacting waves.

Of particular interest in the present study is the effect of salinity, impact surface temperature, and drop diameter and impact velocity (Impact Weber Number) on the spreading of large drops on cold dry surfaces. Towards this end an experimental study was undertaken to examine the physical processes involved with the impacting, spreading and freezing of single drops on cold dry surfaces. These physical processes include the heat transfer to the icing surface, and the effects of surface tension forces and heat transfer on the spreading. This spreading and freezing of drops on cold dry surfaces corresponds to the initial stage of the ice accretion process (i.e. no previously accreted water or ice).

70

4.1 Spreading

Engel (1955) used high speed photography and chemical tracing techniques to examine the collision of large water drops (3 mm in diameter) with a solid surface, at speeds up to terminal velocity. Engel's investigation led to the development of empirical relationships defining the time dependence of the impact force and the radial flow velocity. Savic and Boult also examined the spreading of large drops on warm surfaces. More recently Macklin and Payne (1969) examined the spreading of accreted drops on an ice coated metal cylinder; however they were primarily concerned with conditions typical to atmospheric icing, in particular drops with diameters on the order of 50 μm.

For this study the primary interest was with the marine icing situation, in particular the spreading and freezing of large saline drops. At the present time this author is unaware of any research directed primarily at this marine icing situation. However spreading of large drops on warm surfaces provides a basis of comparison for similar drops spreading and freezing on cold dry surfaces.

4.2 Discussion of Spreading Results

As explained previously (Section 2.6.1), the majority of the results related to the spreading of drops on cold dry surfaces were obtained through the use of high speed video or photographic techniques. These experimental

results provided a means of determining the parameters that best describe the spreading of drops on dry surfaces, namely the spreading rate as a function of time, the initial spreading speed, $S.F._{max}$ and final size ($S.F._{final}$). These parameters were then used as a basis to determine the effects of salinity (S=0 or 33 g/kg), impact surface temperature, drop impact velocity and drop diameter on the spreading process.

The "initial" spreading velocity (V_s) was taken to be the average radial spreading velocity, from the instant of impact until the time t_s. Time t_s is equal to D_d/V_{im}, the time required for the impacting drop to move the distance equal to its diameter. Had there not been resistance to the spreading of the drop, t_s would correspond to the time at which the impact momentum of the spherical drop had been converted into radial momentum of the spreading drop (i.e. complete flattening of the spherical portion of the drop).

Figure 3.3 illustrates graphically the effect of salinity (S=0 or 33 g/kg) on the freezing of drops on a $-20^{\circ}C$ copper surface. The points on the figure correspond to the spreading of 2.4 mm diameters distilled and saline water drops, with impact velocities of 4.8 m/s on the copper surface. The curves on this figure suggest that as a function of time, the spreading size is not strongly dependent on the salinity. Although the lower freezing point of the saline drops allowed the salt water drops to
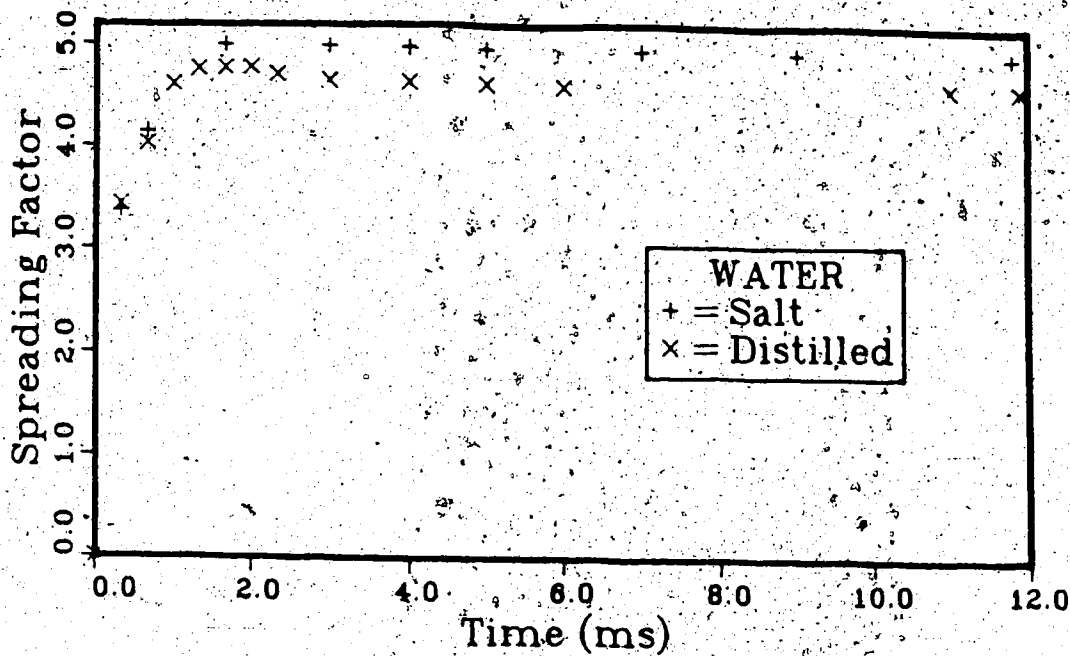
FIGURE 3.3 The effect of salinity on the spreading of 2.4 mm diameter waterdrops on a -20°C copper surface (V_{im} = 4.8 m/s).
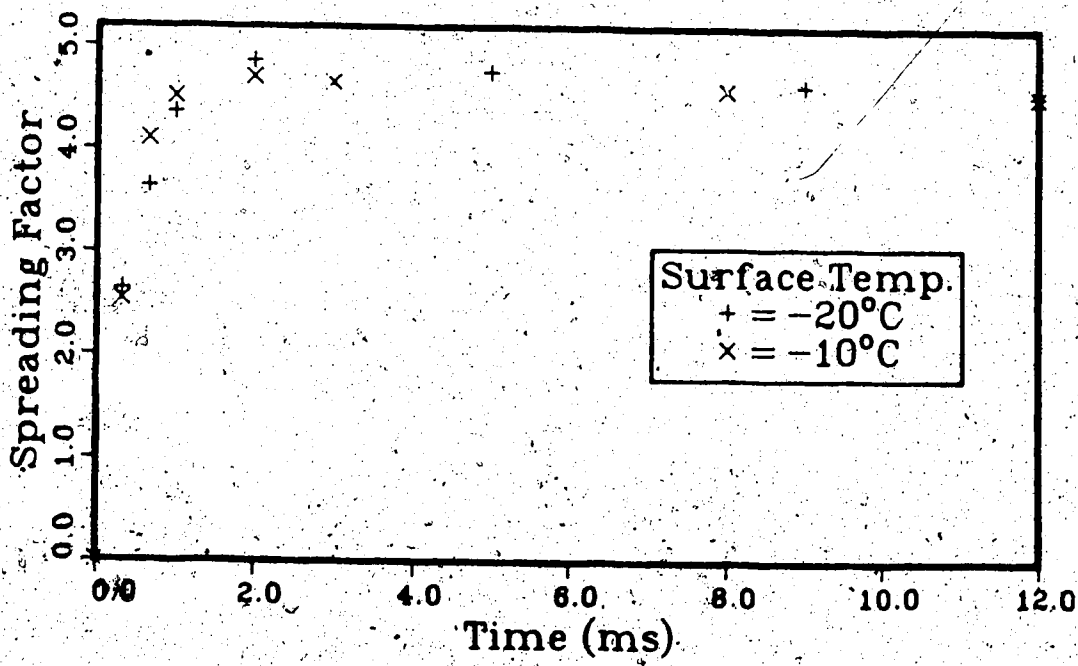

FIGURE 3.4 The effect of impact surface temperature on the spreading of 2.4 mm diameter waterdrops on a stainless steel surface (V_{im}=4.8 m/s).

attain a slightly larger S.F.$_{max}$ ($\approx 4\%$), the curves for the distilled and saline drops are esssentially the same, in terms of spreading rate (i.e. slope) and the final size.

Figure 3.4 illustrates the effect of impact surface temperature on the freezing of 2.4 mm diameter saline water drops on a stainless steel (S.S. 304) plate (V_{im} = 4.8 m/s). For impact surface temperatures of -10 or -20°C, S.F.$_{max}$ was essentially the same (4.86). This would tend to suggest that very little freezing occurs during this initial spreading (up to S.F.$_{max}$). Another indication of this apparent lack of freezing, which can be deduced from both Figures 3.3 and 3.4, is the time required to reached S.F.$_{max}$. For all the drops freezing and spreading on the cold surfaces this time was on the order of 2 ms which is comparable to the corresponding time (2.33 ms) on warm surfaces, as indicated in Figure 3.2.

4.2.1 Maximum Spreading Factor

Calculation of the maximum spreading factor requires a knowledge of the velocity distribution in the spreading drop so as to quantify the energy dissipated by the viscous forces during spreading. Given the complexity of such a calculation and the experimental nature of the present study, such a calculation was not warranted. However, an estimate of an upper limit to the maximum spreading factor can be obtained by considering only the

surface energy of the spread-out drop. To calculate this
surface energy the drop was assumed to spread out as a
disk of uniform thickness and only the energy of the
surface exposed to the air was considered. An estimate of
the S.F.$_{max}$ can then be obtained by equating this surface
energy to the energy of the drop at impact.

The falling drop's energy consists of its kinetic
(KE$_d$), surface (SE$_d$) and gravitional potential energy,
which was excluded since it represented less than 0.1% of
the drop's total energy at impact. The kinetic energy
(KE$_d$) is given by:

$$KE_d = \pi D_d^3 \rho_w V_{im}^2/12 \qquad (4.1)$$

and the spherical drop's surface energy SE$_d$ by:

$$SE_d = \pi D_d^2 \sigma_{a/w} \qquad (4.2)$$

where

D_d = drop diameter (mm)

ρ_w = density of water (kg/m^3)

V_{im} = drop impact velocity (m/s)

$\sigma_{a/w}$ = surface tension - air/water (dynes/cm)

The surface energy of a disk of uniform thickness SE$_{disk}$
is given by:

$$SE_{disk} = A_s \sigma_{a/w} = \pi(D_s^2 + D_s \delta R) \sigma_{a/w} \qquad (4.3)$$

where

δR = thickness of disk (μm)

D_s = diameter of spread out drop (mm)

A_s = drop surface area exposed to air (mm^2)

Equating 4.3 to 4.1 + 4.2 and simplifing:

$$\frac{D_d^3 \, \rho_w \, V_{im}^2}{12 \, \sigma_{a/w}} + D_d^2 = D_s^2 + \frac{D_d^3}{6 \, D_s} \qquad (4.4)$$

Solving equation 4.4 iteratively for D_s gives the results shown in Table 4.1. For 2.4, 1.5 and 1.1 mm drops impacting at 4.8, 4.4 and 4.0 m/s on a warm surface the estimated S.F.$_{max}$ were 8.0, 5.84 and 4.59 as compared to experimental values of 5.38, 4.93 and 4.59 (Table 3.1). These differences indicate the importance of the viscous dissapation in the spreading process. However, this is beyond the scope of the present study; therefore, the subject has been left for future consideration.

Table 3.1 summmarizes the effects of surface temperature and salinity (S=0 or 33 g/kg) on the experimentally determined S.F.$_{max}$ and the time to S.F.$_{max}$. For 2.4 mm diameter distilled drops impacting at 4.8 m/s on a copper surface, the maximum spreading factors were 5.38, 4.85, and 4.76 for copper surfaces maintained at 20, -10 and -20°C, respectively. This trend of decreasing S.F.$_{max}$ with decreases in impact surface temperature was observed for all of the remaining tests using distilled water. For 1.5 mm drops on copper the S.F.$_{max}$ decreased

TABLE 4.1   Maximum spreading factor based on surface
            energy of a disk of uniform thickness, as
            calculated from Equation 4.4.

Drop Diameter D_d (mm)	Impact Velocity V_{im} (m/s)	Spreading Diameter D_s (mm)	Maximum Spreading Factor S.F.$_{max}$
2.4	4.8	19.2	8.0
2.0	4.7	14.64	7.32
1.5	4.4	8.76	5.84
1.1	4.0	5.05	4.59

TABLE 3/1. Effect of impact surface temperature and salinity on the maximum Spreading Factor (S.F.max) and the corresponding time required to reach S.F.max.

| SURFACE | | DROP | | S.F.max | | Time to S.F.max | |
Material	Temp. (°C)	Diameter (mm)	Impact Velocity (m/s)	Distilled	Salt	Distilled (ms)	Salt (ms)
Copper	20	2.4	4.8	5.38	5.38	2.33	2.33
	-10	2.4	4.8	4.85	5.13	2.00	2.00
	-20	2.4	4.8	4.76	5.00	1.33	1.67
	20	1.5	4.4	4.93	4.93	1.20	1.20
	-10	1.5	4.4	4.85	4.69	1.33	1.00
	-20	1.5	4.4	4.12	4.57	0.91	1.00
	20	1.1	4.0	3.91	3.91	0.83	0.83
	-10	1.1	4.0	3.80	—	1.50	—
S.S. 304	-10	2.4	4.8	4.85	4.86	1.55	2.00
	-20	2.4	4.8	4.31	4.86	1.33	2.00
	-10	1.5	4.4	4.49	4.42	1.17	2.00
	-20	1.5	4.4	4.37	4.11	1.16	1.17
Ice	-10	2.4	4.8	5.00	5.40	2.33	2.44
	-20	2.4	4.8	5.15	5.60	1.67	2.33

from 4.93 to 4.85 to 4.12 as the surface temperature was lowered from 20 to -10 to -20°C respectively. Similarly for the 1.1 mm drops the S.F.$_{max}$ decreased from 3.91 to 3.80 as the temperature went from 20 to -10°C. For the saline water drops this trend was still evident; however, the reduction in S.F.$_{max}$ was in general not as large. For the 2.4 mm drops (V$_{im}$ =4.8 m/s) S.F.$_{max}$ decreased from 5.38 to 5.13 to 5.00 and 4.93 to 4.69 to 4.57 for 1.5 mm drops. This may be explained by a simple freezing point depression which allows the drops to attain a slightly larger size before "freezing" becomes a factor.

The effect of surface roughness on S.F.$_{max}$ is illustrated in Table 3.1 through the comparison of the results for the s████████el surface (e = 2.5 μm) to the copper surfa██████████ for all the drops frozen on the copper ████████████was always greater than or equal to ██████████ stainless steel. For S.S. 304 the s█████████ulted in a decrease of 10% in S.F.$_{max}$.█████████he thermal conductivities of the surfaces, if the surfaces had the same roughness the drops would have "frozen" more quickly on the copper surface (i.e. S.F.$_{max}$). Thus the actual decrease in S.F.$_{max}$ due solely to roughness is slightly larger.

The largest S.F.$_{max}$ was obtained for drops freezing on ice surfaces. For a -10°C surface the S.F.$_{max}$ was 5.0 for distilled and 5.4 for 2.4 mm diameter salt water drops and at -20°C, 5.15 and 5.60 respectively. There is some doubt